lecular change in sporadic ALS, does not occur in motor neurons in ALS1 or SBMA. Neurosci Res 54:11–14.

Kuner R, Groom AJ, Bresink I, Kornau HC, Stefovska V, Müller G, Hartmann B, Tschauner K, Waibel S, Ludolph AC, Ikonomidou C, Seeburg PH, Turski L (2005) Late-onset motoneuron disease caused by a functionally modified AMPA receptor subunit. Proc Natl Acad Sci U S A 102: 5826–5831.

Kwak S, Kawahara Y (2005) Deficient RNA editing of GluR2 and neuronal death in amyotropic lateral sclerosis. J Mol Med 83:110–120.

Levanon EY, Eisenberg E, Yelin R, Nemzer S, Hallegger M, Shemesh R, Fligelman ZY, Shoshan A, Pollock SR, Sztybel D, Olshansky M, Rechavi G, Jantsch MF (2004) Systematic identification of abundant A-to-I editing sites in the human transcriptome. Nat Biotechnol 22:1001–1005.

Li JB, Levanon EY, Yoon JK, Aach J, Xie B, Leproust E, Zhang K, Gao Y, Church GM (2009) Genome-wide identification of human RNA editing sites by parallel DNA capturing and sequencing. Science 324:1210–1213.

Lowe JS, Leigh N (2002) Motor neuron disease (amyotrophic lateral sclerosis). In: The Greenfield's neuropathology (Love S, Louis DN, Ellison DW, eds), pp 372–383. Oxford: Oxford UP.

Melcher T, Maas S, Herb A, Sprengel R, Seeburg PH, Higuchi M (1996) A mammalian RNA editing enzyme. Nature 379:460–464.

Misawa H, Nakata K, Toda K, Matsuura J, Oda Y, Inoue H, Tateno M, Takahashi R (2003) VAChT–Cre.Fast and VAChT–Cre.Slow: postnatal expression of Cre recombinase in somatomotor neurons with different onset. Genesis 37:44–50.

Nishimoto Y, Yamashita T, Hideyama T, Tsuji S, Suzuki N, Kwak S (2008) Determination of editors at the novel A-to-I editing positions. Neurosci Res 61:201–206.

Ohmae S, Takemoto-Kimura S, Okamura M, Adachi-Morishima A, Nonaka M, Fuse T, Kida S, Tanji M, Furuyashiki T, Arakawa Y, Narumiya S, Okuno H, Bito H (2006) Molecular identification and characterization of a family of kinases with homology to Ca^{2+}/calmodulin-dependent protein kinases I/IV. J Biol Chem 281:20427–20439.

Paschen W, Hedreen JC, Ross CA (1994) RNA editing of the glutamate receptor subunits GluR2 and GluR6 in human brain tissue. J Neurochem 63:1596–1602.

Paxinos G, Franklin KBJ (2001) The mouse brain in stereotaxic coordinates. San Diego: Academic.

Peng PL, Zhong X, Tu W, Soundarapandian MM, Molner P, Zhu D, Lau L, Liu S, Liu F, Lu Y (2006) ADAR2-dependent RNA editing of AMPA receptor subunit GluR2 determines vulnerability of neurons in forebrain ischemia. Neuron 49:719–733.

Rothstein JD, Martin LJ, Kuncl RW (1992) Decreased glutamate transporter by the brain and spinal cord in amyotrophic lateral sclerosis. N Engl J Med 326:1464–1468.

Sansam CL, Wells KS, Emeson RB (2003) Modulation of RNA editing by functional nucleolar sequestration of ADAR2. Proc Natl Acad Sci U S A 100:14018–14023.

Schymick JC, Talbot K, Traynor BJ (2007) Genetics of sporadic amyotrophic lateral sclerosis. Hum Mol Genet 16 [Spec No 2]:R233–R242.

Seeburg PH (2002) A-to-I editing: new and old sites, functions and speculations. Neuron 35:17–20.

Sommer B, Köhler M, Sprengel R, Seeburg PH (1991) RNA editing in brain controls a determinant of ion flow in glutamate-gated channels. Cell 67:11–19.

Suzuki T, Tsuzuki K, Kameyama K, Kwak S (2003) Recent advances in the study of AMPA receptors. Nippon Yakurigaku Zasshi 122:515–526.

Takemoto-Kimura S, Ageta-Ishihara N, Nonaka M, Adachi-Morishima A, Mano T, Okamura M, Fujii H, Fuse T, Hoshino M, Suzuki S, Kojima M, Mishina M, Okuno H, Bito H (2007) Regulation of dendritogenesis via a lipid-raft-associated Ca^{2+}/calmodulin-dependent protein kinase CLICK-III/CaMKIgamma. Neuron 54:755–770.

Takuma H, Kwak S, Yoshizawa T, Kanazawa I (1999) Reduction of GluR2 RNA editing, a molecular change that increases calcium influx through AMPA receptors, selective in the spinal ventral gray of patients with amyotrophic lateral sclerosis. Ann Neurol 46:806–815.

Van Damme P, Braeken D, Callewaert G, Robberecht W, Van Den Bosch L (2005) GluR2 deficiency accelerates motor neuron degeneration in a mouse model of amyotrophic lateral sclerosis. J Neuropathol Exp Neurol 64:605–612.

Van Den Bosch L, Schwaller B, Vleminckx V, Meijers B, Stork S, Ruehlicke T, Van Houtte E, Klaassen H, Celio MR, Missiaen L, Robberecht W, Berchtold MW (2002) Protective effect of parvalbumin on excitotoxic motor neuron death. Exp Neurol 174:150–161.

Vosler PS, Brennan CS, Chen J (2008) Calpain-mediated signaling mechanisms in neuronal injury and neurodegeneration. Mol Neurobiol 38: 78–100.

Yang JH, Sklar P, Axel R, Maniatis T (1995) Editing of glutamate receptor subunit B pre-mRNA in vitro by site-specific deamination of adenosine. Nature 374:77–81.

Journal of Neurochemistry

JOURNAL OF NEUROCHEMISTRY | 2010 | 115 | 1150–1160 doi: 10.1111/j.1471-4159.2010.07012.x

Ammonium chloride and tunicamycin are novel toxins for dopaminergic neurons and induce Parkinson's disease-like phenotypes in medaka fish

Hideaki Matsui,*,† Hidefumi Ito,* Yoshihito Taniguchi,†,‡,[1] Shunichi Takeda†,‡ and Ryosuke Takahashi*,†

*Department of Neurology, Graduate School of Medicine, Kyoto University, Kyoto, Japan
†Core Research for Evolutional Science and Technology (CREST), Japan Science and Technology Agency, Kawaguchi, Japan
‡Department of Radiation Genetics, Graduate School of Medicine, Kyoto University, Kyoto, Japan

Abstract

Perturbations in protein folding and degradation are key pathological mechanisms in neurodegenerative diseases, including Parkinson's disease (PD). Recent evidence suggests that mishandling of proteins may play an important role in the pathogenesis of PD. We have utilized medaka fish to monitor the effects of injecting neurotoxins into the CSF space. In this study, ammonium chloride, tunicamycin, and lactacystin were tested for their ability to disturb lysosomal proteolysis, N-glycosylation in the endoplasmic reticulum, and proteasomal degradation, respectively. All of the substances tested induced selective loss of dopaminergic neurons, movement disorders and inclusion bodies. Among them, the features of the inclusion bodies that developed after ammonium chloride injection mimicked those of PD: co-localization of ubiquitin and phosphorylated α-synuclein, as well as the presence of LC3 protein in the inclusion bodies. Our study demonstrated that medaka fish are useful for examining the effects of environmental toxins and lysosome inhibition, and lysosome inhibitors may be factors in the development of PD.

Keywords: ammonium chloride, autophagy, lysosome, medaka fish, Parkinson's disease, tunicamycin.

J. Neurochem. (2010) **115**, 1150–1160.

Parkinson's disease (PD) is a neurodegenerative disease that is characterized by motor dysfunction, selective loss of dopaminergic and noradrenergic neurons, and proteinaceous inclusion bodies called Lewy bodies. The etiology of PD is largely unknown, but it has been demonstrated that genetic and environmental factors play a role in the development of the disease (Dauer and Przedborski 2003; Warner and Schapira 2003).

Early animal models developed for PD research utilized dopaminergic neuron-specific toxins such as 6-hydroxydopamine and MPTP (Jonsson 1983; Kopin 1987; Bové *et al.* 2005; Smeyne and Jackson-Lewis 2005; Blandini *et al.* 2008). These classical toxins do not seem to produce inclusion bodies (Schober 2004; Bové *et al.* 2005), although there is one exception: continuous MPTP infusion by minipumps can induce inclusion formation (Fornai *et al.* 2005). More recent models have been generated using general toxins such as paraquat, rotenone or proteasome inhibitors (Brooks *et al.* 1999; Betarbet *et al.* 2000; McNaught *et al.* 2004; Uversky 2004). Rotenone and proteasome inhibitors form inclusion bodies containing ubiquitin and α-synuclein that are similar to Lewy bodies in PD brains (Betarbet *et al.* 2000; McNaught *et al.* 2004). These and other undiscovered toxins for dopaminergic neurons may be related to the etiology of human PD.

Previously, we developed MPTP and proteasome inhibitor models in medaka fish that displayed many features of PD (Matsui *et al.* 2009, 2010b). Medaka fish have proven to be practical for environmental toxin exposure studies because of

Received June 2, 2010; revised manuscript received August 25, 2010; accepted September 7, 2010.

Address correspondence and reprint requests to Dr Takahashi, Department of Neurology, Graduate School of Medicine, Kyoto University, 54 Shogoin-Kawahara-cho, Sakyo-ku, Kyoto 606-8507, Japan. E-mail: ryosuket@kuhp.kyoto-u.ac.jp and Dr Takeda, Department of Radiation Genetics, Graduate School of Medicine, Kyoto University, Yoshida-Konoe-cho, Sakyo-ku, Kyoto 606-8501, Japan.
E-mail: stakeda@rg.med.kyoto-u.ac.jp
[1]The present address of Yoshihito Taniguchi is the Department of Preventive Medicine and Public Health, School of Medicine, Keio University, 35 Shinano-cho, Shinjuku-ku, Tokyo 160-8582, Japan.

Abbreviations used: ER, endoplasmic reticulum; KDEL, Lys-Asp-Glu-Leu; PD, Parkinson's disease; TH, tyrosine hydroxylase.

their small size and the accessibility of their CNS. Using this model system, we report novel toxins for dopaminergic neurons: a lysosome inhibitor, ammonium chloride, and an N-glycosylation inhibitor, tunicamycin.

Materials and methods

Treatment of cells and medaka fish with ammonium chloride, tunicamycin and lactacystin

Ammonium chloride (Wako Pure Chemical, Osaka, Japan), tunicamycin (Nacalai Tesque, Kyoto, Japan) and lactacystin (Kyowa Medex, Tokyo, Japan) were dissolved in 50% dimethylsulfoxide/50% distilled water (v/v). SH-SY5Y cells, from a human dopaminergic cell line, were treated with a vehicle control, 15 mM ammonium chloride, 0.1 μg/mL tunicamycin, or 5 μM lactacystin.

For the treatment of medaka fish, wild-type medaka of the *Kyoto-cab* strain at 10 months post-fertilization were used. Substances were injected into CSF space as previously described (Matsui *et al.* 2010b). Briefly, medaka were anesthetized with chloretone (Tokyo Chemical Industry, Tokyo, Japan). Each fish was moved into an agarose-gel plate with a dent filled with water, then injected with toxins or non-toxic vehicles at a dosage of 0.8 μL/0.1 g body weight. Injections were made using a glass micropipette (GD-1, Narishige, Tokyo, Japan) attached to a Hamilton syringe (Hamilton, Reno, NV, USA). The tip of the glass micropipette was positioned in the CSF space between the hindbrain and the optic tectum. The concentrations of ammonium chloride, tunicamycin, and lactacystin were 100 μg/mL, 100 μg/mL, and 2 mM, respectively.

Enzyme activity assay

The proteasome activity in the medaka brain was measured as previously described (Matsui *et al.* 2010b). Cathepsin D activity was measured using bovine hemoglobin (Sigma Aldrich, St. Louis, MO, USA) as a substrate. Medaka brain was homogenized and sonicated in 200 μL ice-chilled buffer comprised of 1 mM EDTA and 0.2% (v/v) Tween 20 in phosphate-buffered saline. Homogenates were centrifuged at 14 000 *g* for 5 min at 4°C and the supernatant was used for the subsequent assay. The reaction mixture consisted of 100 μL of 2.5% (w/v) hemoglobin, 50 μL of 0.1 M sodium acetate buffer (pH 4.0) and 25 μL of enzyme extract (containing 20 μg of protein). The mixture was incubated for 16 h at 37°C, then 150 μL of 15% (w/v) trichloroacetic acid was added into the mixture. The assay mixture was centrifuged at 20 000 *g* for 5 min at 20°C. The supernatant was neutralized by adding 8% (v/v) 4 M NaOH and the trichloroacetic acid-soluble peptides in the supernatant were measured by the BCA assay kit (Thermo Fischer, Waltham, MA, USA).

Cathepsin H activity was measured using Arg-MCA (methylcoumarin anilide) (Peptide Institute, Osaka, Japan) as a substrate. Medaka brain was homogenized and sonicated in 200 μL ice-chilled buffer comprised of 1 mM EDTA and 0.2% (v/v) Tween 20 in phosphate-buffered saline. Homogenates were centrifuged at 14 000 *g* for 5 min at 4°C and the supernatant was used for the subsequent assay. The reaction mixture consisted of 20 μM of the substrate, 40 mM sodium acetate buffer (pH 4.0) and 10 μL of enzyme extract (containing 10 μg protein). The mixture was incubated for 2 h at 37°C, and then the released AMC (7-amino-4-methylcoumarin) was detected by fluorescence at 460 nm (emission 355 nm) (Fluoroskan Ascent FL, Thermo Fischer).

Western blotting and dot blot analysis

Western blotting was conducted as previously described (Matsui *et al.* 2010a). For dot blot analysis, 3 μL of sample buffer solution was dropped onto the nitrocellulose membrane, and then the membrane was dried for 30 min and subjected to the antigen-antibody reaction. Anti-tyrosine hydroxylase (TH) (1 : 1000, mouse monoclonal, Millipore, Billerica, MA, USA), anti-tryptophan hydroxylase antibody (1 : 1000, sheep polyclonal, Abcam, Cambridge, MA, USA), anti-Lys-Asp-Glu-Leu (KDEL) antibody (1 : 1000, mouse monoclonal, Merck, Darmstadt, Germany), anti-ubiquitin antibody (1 : 1000, rabbit polyclonal, Dako, Glostrup, Denmark), anti-β-actin antibody (1 : 5000, mouse monoclonal, Sigma Aldrich), anti-pan synuclein antibody (1 : 1000, rabbit polyclonal, Millipore), anti-phosphorylated α-synuclein antibody (1 : 1000, mouse monoclonal, Wako Pure Chemical) and anti-oligomer antibody (A11, 1 : 1000, rabbit polyclonal, Invitrogen, Carlsbad, CA, USA) were used for the assay.

Immunohistochemistry and transmission electron microscopy

Immunohistochemistry and transmission electron microscopy were conducted as previously described (Matsui *et al.* 2010b). Anti-phosphorylated α-synuclein antibody (1 : 100, mouse monoclonal, Wako Pure Chemical), anti-pan synuclein antibody (1 : 100, rabbit polyclonal, Millipore), anti-α-synuclein antibody (1 : 100, mouse monoclonal, Invitrogen), anti-LC3 antibody (1 : 100, rabbit polyclonal, MBL, Nagoya, Japan), anti-KDEL antibody (1 : 100, mouse-monoclonal, Merck), anti-ubiquitin antibody (1 : 100 for fluorescence imaging and 1 : 500 for diaminobenzidine (DAB) staining, rabbit polyclonal, Dako) and anti-ubiquitin antibody (1 : 100, mouse monoclonal, Santa Cruz Biotechnology, Santa Cruz, CA, USA) were used for immunohistochemistry.

In vitro kinase reaction of α-synuclein

Four micrograms of recombinant medaka α-synuclein or human α-synuclein was incubated in a buffer containing 25 mM Tris–HCl (pH 7.5), 10 mM $MgCl_2$ and 1 mM ATP with or without 1 unit casein kinase (I or II) (Promega, Madison, WI, USA). The mixture was incubated at 37°C for 1 h. The reaction was stopped by adding sodium dodecyl sulfate sample buffer and boiling at 85°C for 10 min.

Statistical analysis

Data were expressed as means ± standard errors of the mean (SEM). An ANOVA was used to test results for statistical significance. *Post-hoc* analysis using Bonferroni correction for multiple tests was used. Differences were considered significant when $p < 0.05$.

Results

Ammonium chloride, tunicamycin, and lactacystin treatment developed various kinds of inclusions in the human dopaminergic cell line

We first examined whether proteasome inhibition (lactacystin), lysosome inhibition (ammonium chloride), or N-glycosylation inhibition (tunicamycin) could induce

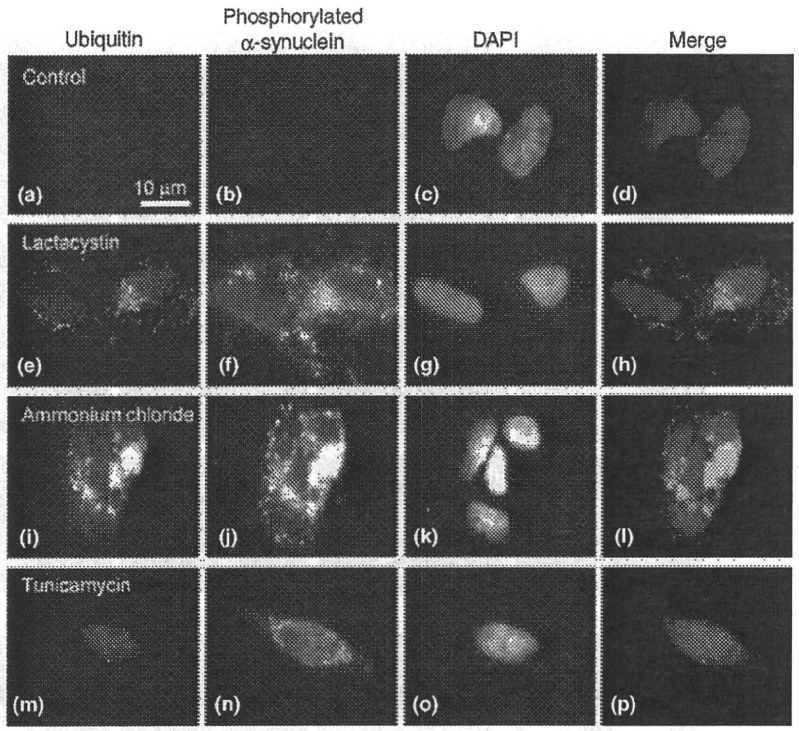

Fig. 1 Ubiquitin and phosphorylated α-synuclein immunocytochemistry of SH-SY5Y cells treated with vehicle control (a–d), lactacystin (e–h), ammonium chloride (i–l), or tunicamycin (m–p) for 48 h. (a, e, i, m) Ubiquitin (green). (b, f, j, n) Phosphorylated α-synuclein (red). (c, g, k, o) DAPI (blue). (d, h, l, p) Merged image of (a)–(c), (e)–(g), (i)–(k), and (m)–(o), respectively.

inclusion formation in the SH-SY5Y human dopaminergic cell line. We stained the cells with anti-ubiquitin and anti-phosphorylated α-synuclein antibody to see the ubiquitin and/or phosphorylated α-synuclein-positive inclusion formation. Two days after treatment, cells treated with any of the three chemicals developed ubiquitin and/or phosphorylated α-synuclein-positive inclusions (Fig. 1e–p), while the vehicle control did not (Fig. 1a–d). However, the staining pattern differed among the groups. In lactacystin-treated SH-SY5Y cells, many inclusions were only ubiquitin or phosphorylated α-synuclein-positive, although some were double-positive (Fig. 1e–h). In contrast, ammonium chloride treatment resulted in inclusions containing both ubiquitin and phosphorylated α-synuclein (Fig. 1i–l). Tunicamycin treatment induced many phosphorylated α-synuclein-positive inclusions but only a few inclusions contained ubiquitin (Fig. 1m–p). These results were also reproduced when using anti-α-synuclein antibody (Figure S1a–p).

We hypothesized that these inclusion bodies contain different proteins as a result of the toxin that was used. Ammonium chloride inhibits lysosome-autophagosome fusion, which should lead to an accumulation of markers for autophagosomes. On the other hand, tunicamycin induces protein misfolding in the endoplasmic reticulum (ER), which may result in inclusion bodies containing ER proteins. As predicted, ubiquitin-positive inclusion bodies that developed after treatment with ammonium chloride contained LC3, a marker for autophagosomes (Fig. 2A–P). Inclusion bodies expressing this marker did not result from treatment with lactacystin or tunicamycin. Inclusion bodies in tunicamycin-treated cells, and not in lactacystin- or ammonium chloride-treated cells, contained KDEL, a signal sequence for ER chaperones (Fig. 2Q–f).

In summary, ammonium chloride (a lysosome inhibitor), tunicamycin (an N-glycosylation inhibitor), and lactacystin (a proteasome inhibitor) developed inclusion bodies in SH-SY5Y cells with different characteristics according to the toxin used.

Ammonium chloride and tunicamycin developed ubiquitin-positive inclusions in medaka brain

Next, to examine the effects of ammonium chloride, tunicamycin, or lactacystin in *in vivo* animal models, we administered these substances into medaka CSF using the method previously described (Matsui *et al.* 2010b). At first, we measured lysosome activity (cathepsin D/H activity), ER stress (KDEL expression level), and proteasome activity of medaka brains to check the specific effects of these toxins in medaka whole brain. Cathepsin D/H activity appeared to be up-regulated in ammonium chloride-treated brains, probably because of compensation (Figure S2a and b). KDEL expression was increased in tunicamycin-treated brains, indicating successful induction of ER stress in these brains (Figure S2c). Proteasome activity was decreased in lactacystin-treated brains as previously described (data not shown, Matsui *et al.* 2010b). These data indicate that each chemical induced specific effects in medaka brains *in vivo*.

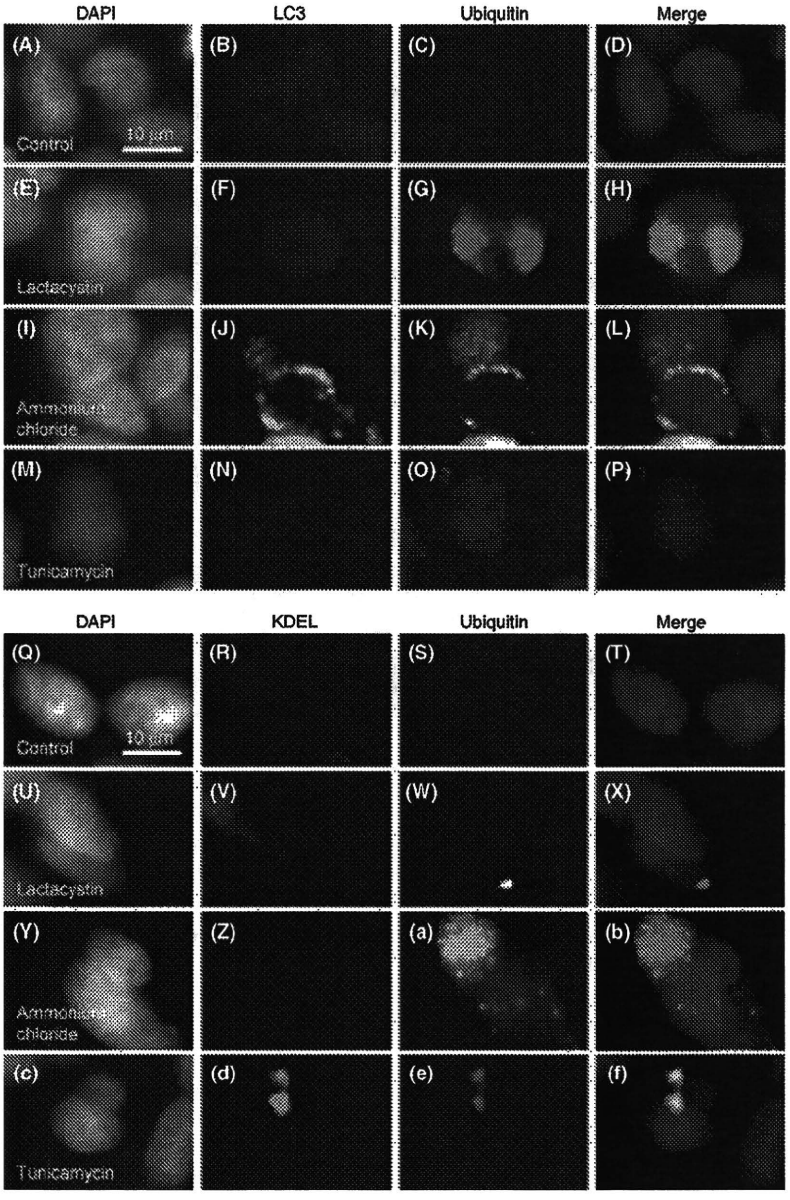

Fig. 2 Ubiquitin, LC3 and KDEL immunocytochemistry of SH-SY5Y cells treated with vehicle control, ammonium chloride, tunicamycin, or lactacystin for 48 h (A-f). (A–D) Vehicle control. (E–H) Lactacystin. (I–L) Ammonium chloride. (M–P) Tunicamycin. (A, E, I, M) DAPI. (B, F, J, N) LC3. (C, G, K, O) Ubiquitin. (D, H, L, P) Merged image of (A)–(C), (E)–(G), (I)–(K), and (M)–(O), respectively. (Q–T) Vehicle control. (U–X) Lactacystin. (Y–b) Ammonium chloride. (c–f) Tunicamycin. (Q, U, Y, c) DAPI. (R, V, Z, d) KDEL. (S, W, a, e) Ubiquitin. (T, X, b, f) Merged image of (Q)–(S), (U)–(W), (Y)–(a), and (c)–(e), respectively.

Western blotting of medaka brains showed increased amounts of ubiquitin binding proteins following ammonium chloride, tunicamycin, or lactacystin injection compared to the vehicle control (Fig. 3a and b, Matsui *et al.* 2010b). To test whether treatment with ammonium chloride, tunicamycin, or lactacystin resulted in an increase in inclusion bodies in medaka brain, we stained brain sections with an anti-ubiquitin antibody. Three days after administration of ammonium chloride, tunicamycin, or lactacystin, ubiquitin-positive cytoplasmic inclusions were seen in the brain as well as in TH-positive dopaminergic neurons (Fig. 3c–h, Matsui *et al.* 2010b). Treatment with the vehicle did not result in the formation of inclusion bodies (Fig. 3c and f).

Collectively, both ammonium chloride and tunicamycin induced ubiquitin-positive inclusion bodies in medaka brain similar to those induced by the proteasome inhibitors lactacystin and epoxomicin (Matsui *et al.* 2010b).

Ammonium chloride and tunicamycin induce selective loss of dopaminergic/noradrenergic neurons in medaka fish

We previously described that the proteasome inhibitors lactacystin and epoxomicin developed not only ubiquitin-positive inclusions but also other PD-like phenotypes such as selective loss of dopaminergic/noradrenergic neurons and movement disorder (Matsui *et al.* 2010b). To assess whether ammonium chloride or tunicamycin also cause PD-like phenotypes, we performed western blotting,

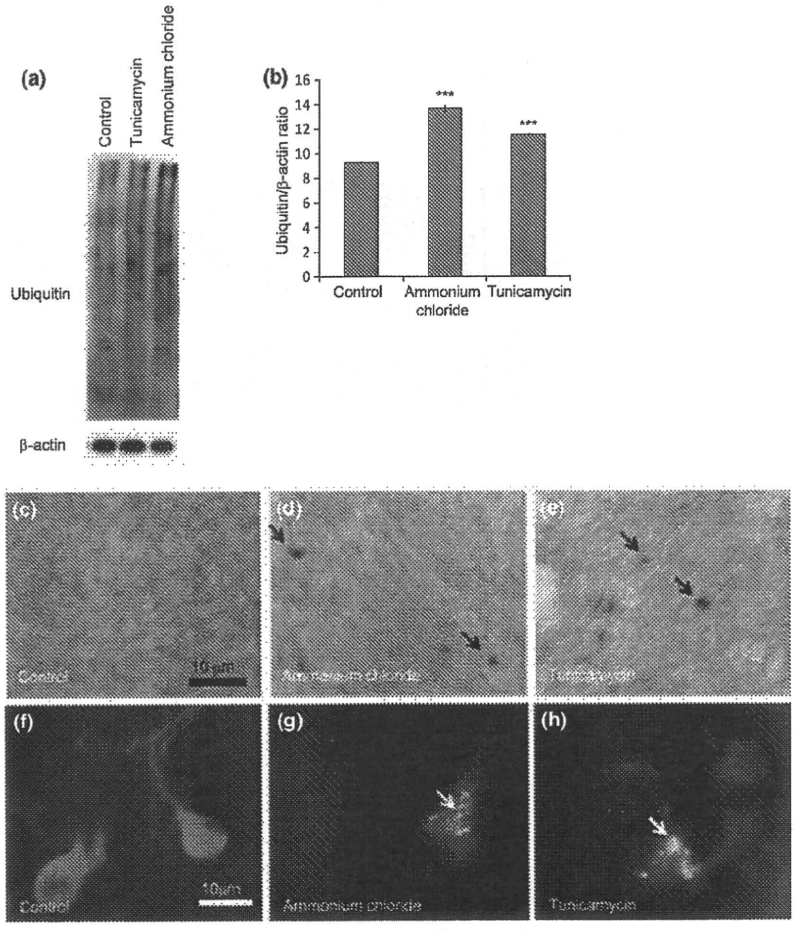

Fig. 3 Ubiquitin immunohistochemistry and western blotting of medaka brains treated with vehicle control, ammonium chloride, tunicamycin for 3 days. (a) Western blotting of ubiquitin and β-actin of the brains. (b) Densitometric analysis of the western blotting. ***$p < 0.001$ vs. control. (c–e) Anti-ubiquitin antibody staining (DAB staining). (f–h) Anti-ubiquitin (green) and anti-TH (red) antibodies staining (fluorescence imaging). (c, f) Control brain. (d, g) Ammonium chloride-treated brain. (e, h) Tunicamycin-treated brain. Arrows indicate ubiquitin-positive inclusion bodies.

immunohistochemical analysis, HPLC and behavioral assays. Western blotting of medaka whole brain revealed a reduction in TH, a marker of dopaminergic/noradrenergic neurons, in ammonium chloride and tunicamycin-treated medaka fish (Figure S3a and b). Tryptophan hydroxylase, a marker for serotoninergic neurons, did not differ among these groups, indicating selective loss of TH in these brains (Figure S3a). Similar to the case of proteasome inhibitors, ammonium chloride and tunicamycin treatment reduced TH-positive dopaminergic neurons in the middle diencephalon (a possible equivalent of the substantia nigra in mammals) and TH-positive noradrenergic neurons in the medulla oblongata (Fig. 4a–m). Nissl-positive neurons in the optic tectum were not reduced, further indicating selective loss of TH-positive neurons (Fig. 4n). To evaluate whether these substances induced apoptosis, we conducted TdT-mediated dUTP-biotin nick end labeling (TUNEL) assay using the methods previously described (Matsui *et al.* 2010a). In the middle diencephalon of ammonium chloride-treated and tunicamycin-treated medaka brain, TdT-mediated dUTP-biotin nick end labeling (TUNEL) and TH double-labeled cells were observed (Fig. 4o–v), but they were not observed in vehicle-treated cells. These findings indicate that ammonium chloride and tunicamycin treatment indeed induced cell death of TH-positive neurons in the middle diencephalon, at least partly by apoptosis. To measure the amount of catecholamine species, medaka whole brain was subjected to HPLC analysis. Results show a reduction in dopamine and noradrenaline but not in serotonin, providing further evidence of selective loss of dopaminergic/noradrenergic neurons following ammonium chloride and tunicamycin treatment (Figure S4a–c). Finally, we traced and analyzed the swimming behavior of medaka fish using the method previously described (Matsui *et al.* 2010b). The behavioral assay showed a decrease in spontaneous swimming movement in ammonium chloride- and tunicamycin-treated medaka fish (Figure S5a–c).

In summary, ammonium chloride and tunicamycin treatment caused selective loss of dopaminergic/noradrenergic neurons and movement disorder, similar to human PD.

Ammonium chloride, tunicamycin, and lactacystin showed different kinds of inclusion bodies in the brain of medaka fish

Because Lewy bodies are known to contain not only ubiquitin but also phosphorylated α-synuclein, we stained

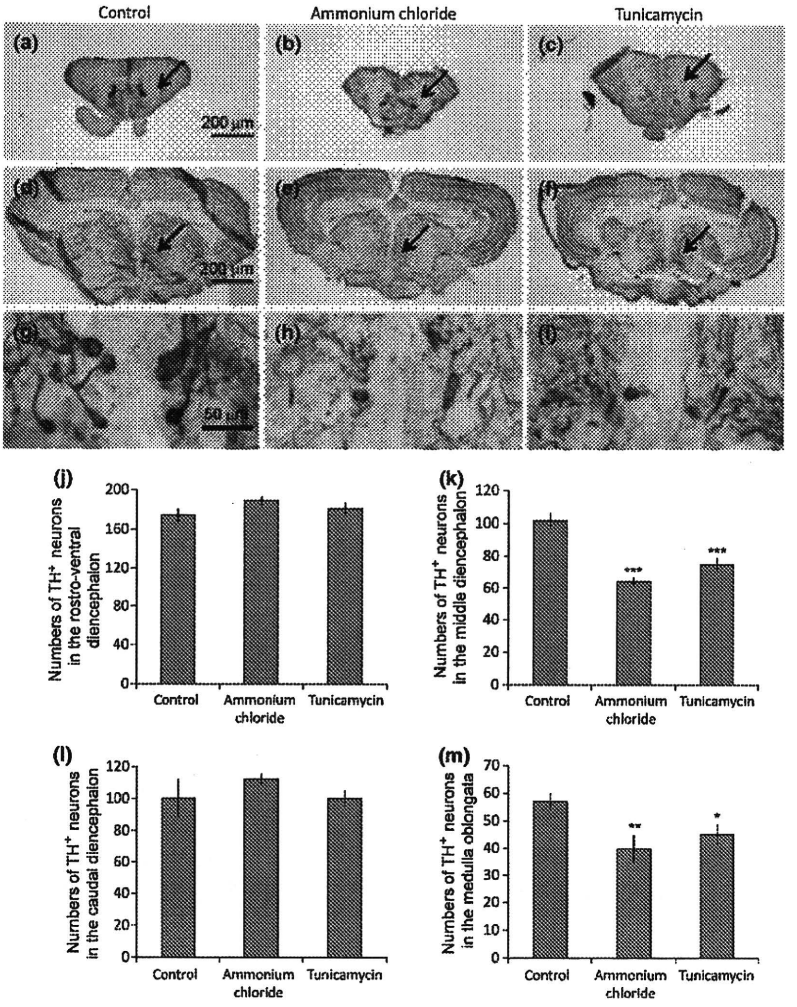

Fig. 4 Anti-TH antibody and TUNEL staining of vehicle control-, ammonium chloride-, and tunicamycin-treated brain sections. (a–c) TH-positive fibers (arrows) in the forebrain. (d–f) TH-positive neurons (arrows) in the middle diencephalon. (g–i) Enlarged images of (d)–(f), respectively. (a, d, g) Control brains. (b, e, h) Ammonium chloride-treated brains. (c, f, i) Tunicamycin-treated brains. (j–m) Numbers of TH-positive neurons in the rostro-ventral diencephalon (j), middle diencephalon (k), caudal diencephalon (l) and medulla oblongata (m). $^{***}p < 0.001$, $^{**}p < 0.01$, $^{*}p < 0.05$ vs. control ($n = 6$). (n) Number of Nissl-positive neurons in the optic tectum ($n = 6$). (o–r) Ammonium chloride-treated brain. (s–v) Tunicamycin-treated brain. (o, s) DAPI staining. (p, t) Anti-TH antibody staining. (q, u) TUNEL staining. (r, v) Merged image of (o)–(q) and (s)–(u), respectively. Arrows indicate TUNEL-positive TH neurons in the middle diencephalon.

medaka brains with anti-phosphorylated α-synuclein antibody. We first tested whether anti-phosphorylated α-synuclein antibody binds to phosphorylated medaka α-synuclein. Phosphorylated medaka α-synuclein was produced by *in vitro* kinase reaction with recombinant medaka α-synuclein and casein kinase I or II. Dot blot analysis showed that anti-phosphorylated α-synuclein antibody reacted with phosphorylated human and medaka α-synuclein but not with non-phosphorylated human and medaka α-synuclein (Figure S6a).

Next, we performed western blotting of medaka whole brain using this anti-phosphorylated α-synuclein antibody. The result showed an increased amount of high molecular weight bands in tunicamycin- and ammonium chloride-treated fish (Figure S6b). Anti-oligomer specific antibody disclosed increased immunochemical signals in these fish, indicating increased amount of α-synuclein oligomer in tunicamycin- and ammonium chloride-treated fish (Figure S6c). Immunohistochemical analysis showed that ammonium chloride, tunicamycin, and lactacystin treatment increased ubiquitin-positive inclusions while vehicle control did not. Ammonium chloride- and tunicamycin-treated brain also revealed an increased amount of phosphorylated α-synuclein-positive inclusions, but such inclusions were not found in lactacystin- or vehicle-treated groups (Fig. 5a–r). Pre-absorption by medaka phosphorylated α-synuclein diminished the signals of anti-phosphorylated α-synuclein antibody, indicating that this antibody indeed recognized medaka phosphorylated α-synuclein (Fig. 5m–o). Co-localization of ubiquitin and phosphorylated α-synuclein was not seen in vehicle-, tunicamycin-, or lactacystin-treated medaka, but several inclusions in ammonium chloride-treated brain were both ubiquitin- and phosphorylated α-synuclein-positive (Fig. 5a–r). This co-localization was also demonstrated when using anti-α-synuclein and anti-ubiquitin antibodies (Figure S7a–l).

We next examined whether these inclusion bodies contain LC3 or KDEL proteins. Inclusion bodies caused by lactacystin did not contain LC3 or KDEL. However, inclusion bodies in ammonium chloride-treated brains exhibited both anti-ubiquitin and anti-LC3 immunoreactivity.

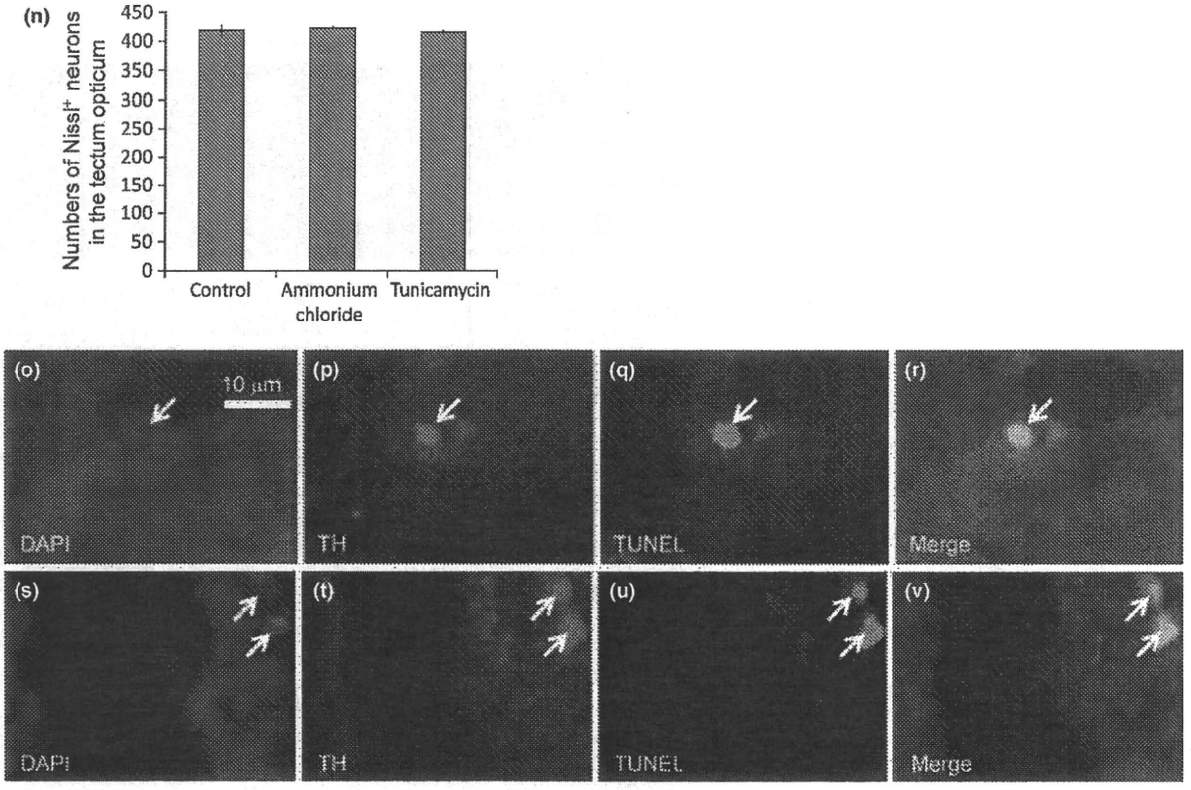

Fig. 4 *Continued.*

Tunicamycin-treated samples also revealed inclusion bodies that contained both ubiquitin and KDEL (Fig. 6a–r).

Finally, we used transmission electron microscopy to examine the detailed structure of the inclusions. Aggregates with multiple concentric and filamentous structures were observed in the cytoplasm in ammonium chloride-treated medaka brain (Fig. 7a and b). The brain also contained abnormal lysosome-related structures containing whorled membranous material, which were not seen in the vehicle control (Fig. 7c and d). Tunicamycin-treated medaka brain showed abnormal structures containing vacuoles and electron-dense materials (Fig. 7e and f). The brain also contained abnormal lysosome-related structures containing whorled membranous material similar to ammonium chloride samples (Fig. 7g and h).

In conclusion, ammonium chloride, tunicamycin, and lactacystin treatment resulted in the development of various kinds of inclusion bodies, and the characteristics of these inclusion bodies differed depending on the toxins.

Discussion

In this report, we described that ammonium chloride and tunicamycin caused selective loss of dopaminergic/noradrenergic neurons, movement disorders and inclusion bodies similar to proteasome inhibitor models we previously reported. Although these toxins shared many features of PD, the specific characteristics of the inclusion bodies were dependent on the toxin used.

In Lewy bodies associated with PD, α-synuclein, the protein responsible for familial autosomal dominant PD (Polymeropoulos *et al.* 1997), is phosphorylated and accumulates with ubiquitin (Spillantini *et al.* 1997; Iwatsubo 2003). A recent paper demonstrated that brain samples from α-synuclein transgenic mice and patients with Lewy body disease also showed LC3-positive inclusion bodies (Crews *et al.* 2010). Among the toxins we tested, ammonium chloride seems to better replicate the features typical of Lewy bodies such as co-localization of phosphorylated α-synuclein and ubiquitin, and the presence of LC3 protein in inclusions.

A central issue in the pathogenesis of neurodegeneration is the disturbance of protein folding, aggregation and degradation. There are two major pathways for protein degradation, the ubiquitin-proteasome system and the autophagy–lysosome systems (Ciechanover 2005). Recent evidence suggests an association between PD pathogenesis and autophagy–lysosome systems. Lysosomal clearance has been shown to be disrupted by α-synuclein, which has effects on chaperone-mediated autophagy (Cuervo *et al.*

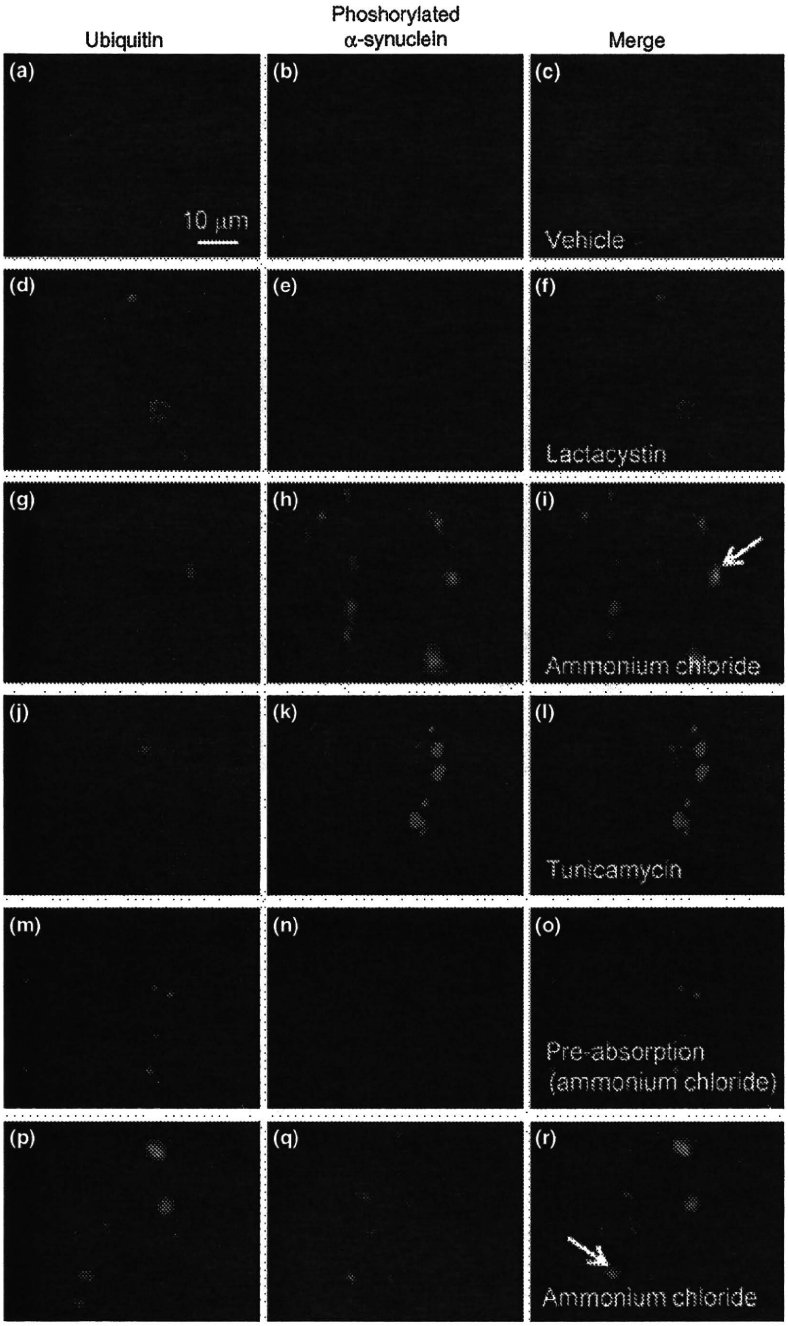

Fig. 5 Ubiquitin and phosphorylated α-synuclein immunohistochemistry of medaka brains. (a–c) Vehicle control. (d–f) Lactacystin-treated brain. (g–i) Ammonium chloride-treated brain. (j–l) Tunicamycin-treated brain. (m–o) Ammonium chloride-treated brain with anti-phosphorylated α-synuclein antibody pre-absorbed by medaka phosphorylated α-synuclein (10 μg/mL). (p–r) Additional examples of ammonium chloride-treated brain. (a, d, g, j, m, p) Anti-ubiquitin antibody staining. (b, e, h, k, n, q) Anti-phosphorylated α-synuclein antibody staining. (c, f, i, l, o, r) Merged image of (a) and (b), (d) and (e), (g) and (h), (j) and (k), (m) and (n), and (p) and (q), respectively. Arrows indicate ubiquitin and phosphorylated α-synuclein double-positive cells.

2004). Previous studies have shown that lysosome storage diseases such as Gaucher disease and Niemann-Pick disease often develop parkinsonism and α-synuclein accumulation (Tayebi *et al.* 2001; Várkonyi *et al.* 2003; Saito *et al.* 2004). Furthermore, there is now increasing evidence that *parkin* and *PINK1*, genes responsible for autosomal recessive familial PD, play important roles in mitophagy (mitochondria-specific autophagy) and lysosomal clearance of mitochondria (Narendra *et al.* 2008, 2010; Geisler *et al.* 2010; Kawajiri *et al.* 2010; Matsuda *et al.* 2010; Michiorri *et al.* 2010; Vives-Bauza *et al.* 2010). Mouse embryonic fibroblasts deficient in *DJ-1*, another gene responsible for autosomal recessive PD, also showed lysosomal pathology (Krebiehl *et al.* 2010). Furthermore, *Atg7*-deficient mice show neurodegeneration and inclusion bodies similar to Lewy bodies (Komatsu *et al.* 2006). Our results are consistent with prior studies and provide further support for the idea that lysosome inhibition can cause PD.

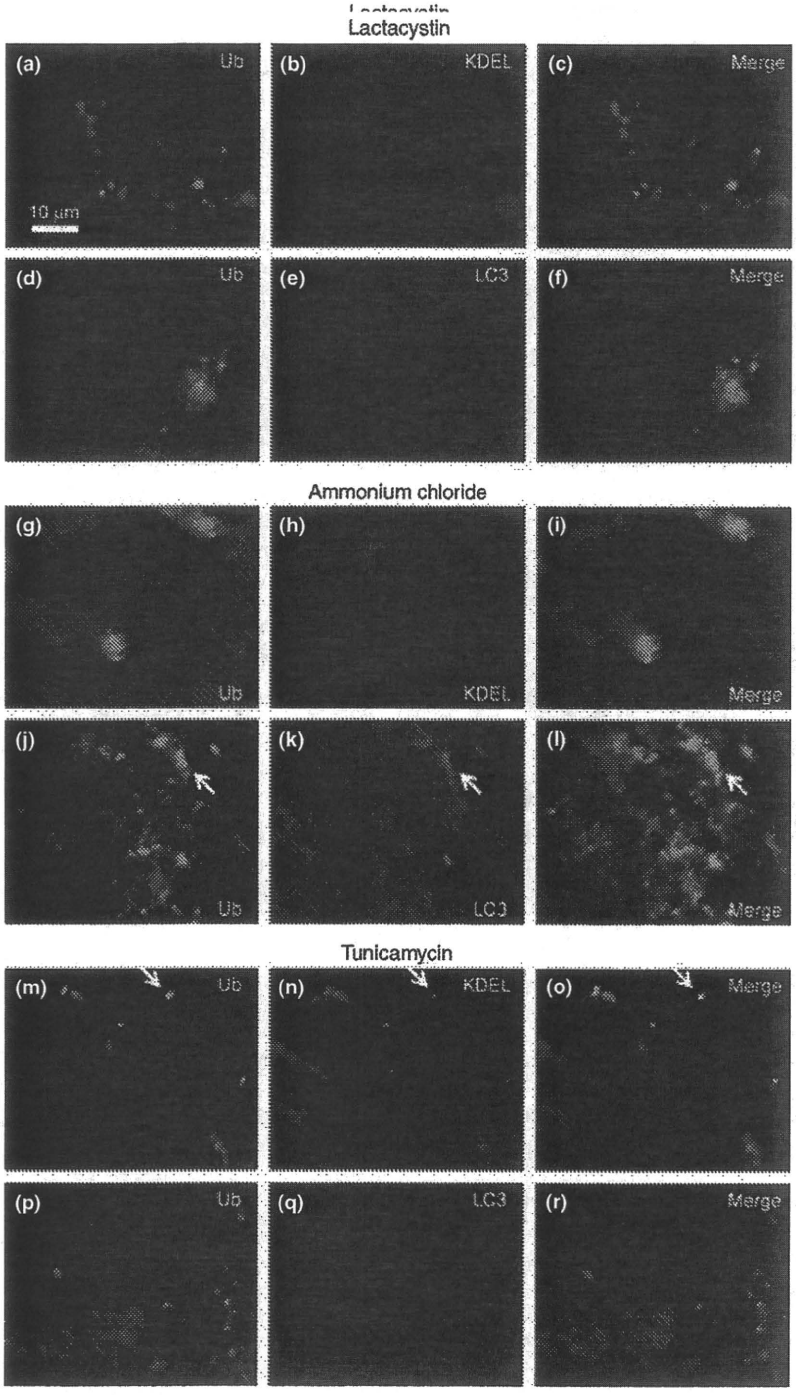

Fig. 6 Anti-ubiquitin, KDEL, LC3 antibody staining of lactacystin-, ammonium chloride-, and tunicamycin-treated brains. (a–f) Lactacystin-treated brain. (g–l) Ammonium chloride-treated brain. (m–r) Tunicamycin-treated brain. (a, d, g, j, m, p) Anti-ubiquitin antibody staining. (b, h, n) Anti-KDEL staining. (e, k, q) Anti-LC3 staining. (c, f, i, l, o, r) Merged image of (a) and (b), (d) and (e), (g) and (h), (j) and (k), (m) and (n), and (p) and (q), respectively. Arrows indicate an example of ubiquitin/KDEL or ubiquitin/LC3 double-positive cells.

Ammonium chloride has been reported to elevate pH in the lysosome and inhibit phagosome-lysosome fusion (Ohkuma and Poole 1981). This substance can be found naturally in volcanic regions, forming on volcanic rocks near fume-releasing vents. Ammonium chloride is widely used in everyday applications, including cleaning the tip of soldering irons and can also be included in the soldering iron itself. Ammonium chloride is a common ingredient in hair shampoo, textile printing, plywood glue, and some alcoholic drinks. Because ammonium chloride and other substances that inhibit lysosomal function may be related to the etiology of PD, we must examine environmental lysosome inhibitors in general as pathogenic candidates for PD.

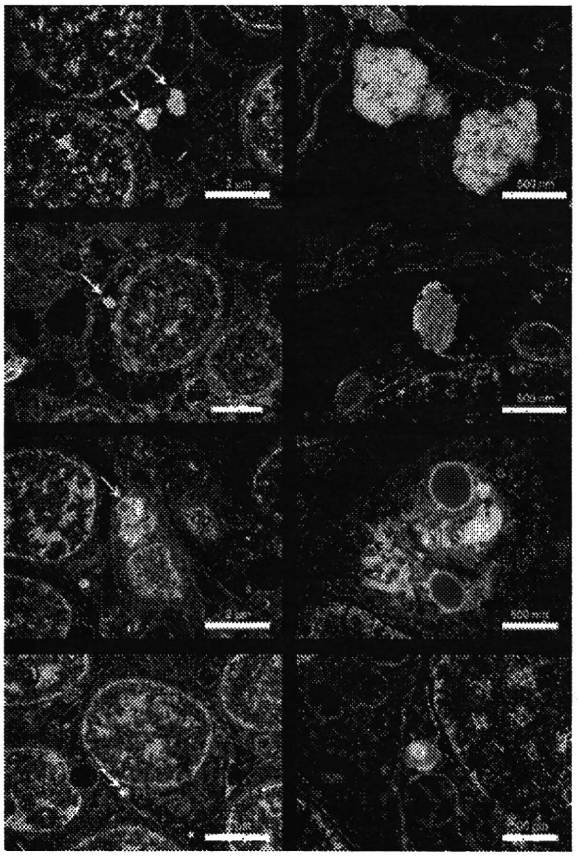

Fig. 7 Transmission electron microscopic image of ammonium chloride- and tunicamycin-treated brains. (a) Aggregates containing filamentous structures in ammonium chloride-treated brain (arrows). (b) Enlarged image of (a). (c) Abnormal lysosome-related structure containing membranous structures (arrow). (d) Enlarged image of (c). (e) Abnormal structure containing electron dense materials and vacuoles in tunicamycin-treated brain (arrow). (f) Enlarged image of (e). (g) Abnormal lysosome-related structure containing membranous structures (arrow). (h) Enlarged image of (g).

In conclusion, several agents that cause mishandling of proteins can induce PD-like phenotypes. Among the substances we tested, ammonium chloride can replicate Lewy body-like inclusions and may be related to the pathogenesis of PD. Further studies are needed to examine the relationship between lysosomal dysfunction and PD, especially the possibility of lysosome inhibitors as an environmental risk factor.

Acknowledgement

We wish to thank the Kondoh Differentiation Signaling Project, JST, for permission to use *Kyoto-cab* strain medaka fish. We are grateful to Ai Tanigaki and Dr. Roberto Gavinio, who supported our experiments and English editing, respectively. We are also grateful to Satoshi Fukui for the assistance with our electron microscopy studies.

Supporting information

Additional Supporting Information may be found in the online version of this article:

Figure S1. Ubiquitin and α-synuclein immunocytochemistry of SH-SY5Y cells treated with vehicle control (a–d), lactacystin (e–h), ammonium chloride (i–l), or tunicamycin (m–p) for 48 h.

Figure S2. Effects of ammonium chloride, tunicamycin, and lactacystin on whole medaka brain.

Figure S3. TH/TPH (tryptophan hydroxylase) western blotting of medaka whole brains treated with vehicle control, ammonium chloride and tunicamycin.

Figure S4. HPLC analysis of catecholamine in vehicle control-, ammonium chloride-, and tunicamycin-treated medaka brain (n = 6).

Figure S5. Spontaneous swimming movement of vehicle control-, ammonium chloride-, and tunicamycin-treated medaka (n = 9).

Figure S6. Western blotting of anti-phosphorylated α-synuclein antibody in vehicle control-, ammonium chloride-, tunicamycin-, and lactacystin-treated brains.

Figure S7. Ubiquitin and synuclein immunohistochemistry of medaka brains.

As a service to our authors and readers, this journal provides supporting information supplied by the authors. Such materials are peer-reviewed and may be re-organized for online delivery, but are not copy-edited or typeset. Technical support issues arising from supporting information (other than missing files) should be addressed to the authors.

References

Betarbet R., Sherer T. B., MacKenzie G., Garcia-Osuna M., Panov A. V. and Greenamyre J. T. (2000) Chronic systemic pesticide exposure reproduces features of Parkinson's disease. *Nat. Neurosci.* **3**, 1301–1306.

Blandini F., Armentero M. T. and Martignoni E. (2008) The 6-hydroxydopamine model: news from the past. *Parkinsonism Relat. Disord.* **14**(Suppl 2), S124–S129.

Bové J., Prou D., Perier C. and Przedborski S. (2005) Toxin-induced models of Parkinson's disease. *NeuroRx* **2**, 484–494.

Brooks A. I., Chadwick C. A., Gelbard H. A., Cory-Slechta D. A. and Federoff H. J. (1999) Paraquat elicited neurobehavioral syndrome caused by dopaminergic neuron loss. *Brain Res.* **823**, 1–10.

Ciechanover A. (2005) Proteolysis: from the lysosome to ubiquitin and the proteasome. *Nat. Rev. Mol. Cell Biol.* **6**, 79–87.

Crews L., Spencer B., Desplats P., Patrick C., Paulino A., Rockenstein E., Hansen L., Adame A., Galasko D. and Masliah E. (2010) Selective molecular alterations in the autophagy pathway in patients with Lewy body disease and in models of alpha-synucleinopathy. *PLoS ONE* **5**, e9313.

Cuervo A. M., Stefanis L., Fredenburg R., Lansbury P. T. and Sulzer D. (2004) Impaired degradation of mutant alpha-synuclein by chaperone-mediated autophagy. *Science* **305**, 1292–1295.

Dauer W. and Przedborski S. (2003) Parkinson's disease: mechanisms and models. *Neuron* **39**, 889–909.

Fornai F., Schlüter O. M., Lenzi P. *et al.* (2005) Parkinson-like syndrome induced by continuous MPTP infusion: convergent roles of the ubiquitin-proteasome system and alpha-synuclein. *Proc. Natl Acad. Sci. USA* **102**, 3413–3418.

Geisler S., Holmström K. M., Skujat D., Fiesel F. C., Rothfuss O. C., Kahle P. J. and Springer W. (2010) PINK1/Parkin-mediated

mitophagy is dependent on VDAC1 and p62/SQSTM1. *Nat. Cell Biol.* **12**, 119–131.

Iwatsubo T. (2003) Aggregation of alpha-synuclein in the pathogenesis of Parkinson's disease. *J. Neurol.* **250**(Suppl 3), III11–III14.

Jonsson G. (1983) Chemical lesioning techniques: monoamine neurotoxins, in *Handbook of Chemical Neuroanatomy. Methods in Chemical Neuroanatomy* (Björklund A. and Hökfelt T., eds), Edn 1, Vol. 1, pp. 463–507. Elsevier Science Publishers B.V, Amsterdam.

Kawajiri S., Saiki S., Sato S., Sato F., Hatano T., Eguchi H. and Hattori N.. (2010) PINK1 is recruited to mitochondria with parkin and associates with LC3 in mitophagy. *FEBS Lett.* **584**, 1073–1079.

Komatsu M., Waguri S., Chiba T. *et al.*(2006) Loss of autophagy in the central nervous system causes neurodegeneration in mice. *Nature* **441**, 880–884.

Kopin I. J. (1987) MPTP: an industrial chemical and contaminant of illicit narcotics stimulates a new era in research on Parkinson's disease. *Environ. Health Perspect.* **75**, 45–51.

Krebiehl G., Ruckerbauer S., Burbulla L. F. *et al.* (2010) Reduced basal autophagy and impaired mitochondrial dynamics due to loss of Parkinson's disease-associated protein DJ-1. *PLoS ONE* **5**, e9367.

Matsuda N., Sato S., Shiba K. *et al.* (2010) PINK1 stabilized by mitochondrial depolarization recruits Parkin to damaged mitochondria and activates latent Parkin for mitophagy. *J. Cell Biol.* **189**, 211–221.

Matsui H., Taniguchi Y., Inoue H., Uemura K., Takeda S. and Takahashi R. (2009) A chemical neurotoxin, MPTP induces Parkinson's disease like phenotype, movement disorders and persistent loss of dopamine neurons in medaka fish. *Neurosci. Res.* **65**, 263–271.

Matsui H., Taniguchi Y., Inoue H., Kobayashi Y., Sakaki Y., Toyoda A., Uemura K., Kobayashi D., Takeda S. and Takahashi R. (2010a) Loss of PINK1 in medaka fish (Oryzias latipes) causes late-onset decrease in spontaneous movement. *Neurosci. Res.* **66**, 151–161.

Matsui H., Ito H., Taniguchi Y., Inoue H., Takeda S. and Takahashi R. (2010b) Proteasome inhibition in medaka brain induces the features of Parkinson disease. *J. Neurochem.* **115**, 178–187.

McNaught K. S., Perl D. P., Brownell A. L. and Olanow C. W. (2004) Systemic exposure to proteasome inhibitors causes a progressive model of Parkinson's disease. *Ann. Neurol.* **56**, 149–162.

Michiorri S., Gelmetti V., Giarda E. *et al.* (2010) The Parkinson-associated protein PINK1 interacts with Beclin1 and promotes autophagy. *Cell Death Differ.* **17**, 962–974.

Narendra D., Tanaka A., Suen D. F. and Youle R. J. (2008) Parkin is recruited selectively to impaired mitochondria and promotes their autophagy. *J. Cell Biol.* **183**, 795–803.

Narendra D. P., Jin S. M., Tanaka A., Suen D. F., Gautier C. A., Shen J., Cookson M. R. and Youle R. J. (2010) PINK1 is selectively stabilized on impaired mitochondria to activate Parkin. *PLoS Biol.* **8**, e1000298.

Ohkuma S. and Poole B. (1981) Cytoplasmic vacuolation of mouse peritoneal macrophages and the uptake into lysosomes of weakly basic substances. *J. Cell Biol.* **90**, 656–664.

Polymeropoulos M. H., Lavedan C., Leroy E. *et al.* (1997) Mutation in the alpha-synuclein gene identified in families with Parkinson's disease. *Science* **276**, 2045–2047.

Saito Y., Suzuki K., Hulette C. M. and Murayama S. (2004) Aberrant phosphorylation of alpha-synuclein in human Niemann-Pick type C1 disease. *J. Neuropathol. Exp. Neurol.* **63**, 323–328.

Schober A. (2004) Classic toxin-induced animal models of Parkinson's disease: 6-OHDA and MPTP. *Cell Tissue Res.* **318**, 215–224.

Smeyne R. J. and Jackson-Lewis V. (2005) The MPTP model of Parkinson's disease. *Brain Res. Mol. Brain Res.* **134**, 57–66.

Spillantini M. G., Schmidt M. L., Lee V. M., Trojanowski J. Q., Jakes R. and Goedert M. (1997) Alpha-synuclein in Lewy bodies. *Nature* **388**, 839–840.

Tayebi N., Callahan M., Madike V., Stubblefield B. K., Orvisky E., Krasnewich D., Fillano J. J. and Sidransky E. (2001) Gaucher disease and parkinsonism: a phenotypic and genotypic characterization. *Mol. Genet. Metab.* **73**, 313–321.

Uversky V. N. (2004) Neurotoxicant-induced animal models of Parkinson's disease: understanding the role of rotenone, maneb and paraquat in neurodegeneration. *Cell Tissue Res.* **318**, 225–241.

Várkonyi J., Rosenbaum H., Baumann N., MacKenzie J. J., Simon Z., Aharon-Peretz J., Walker J. M., Tayebi N. and Sidransky E. (2003) Gaucher disease associated with parkinsonism: four further case reports. *Am. J. Med. Genet. A* **116**, 348–351.

Vives-Bauza C., Zhou C., Huang Y. *et al.* (2010) PINK1-dependent recruitment of Parkin to mitochondria in mitophagy. *Proc. Natl Acad. Sci. USA* **107**, 378–383.

Warner T. T. and Schapira A. H. (2003) Genetic and environmental factors in the cause of Parkinson's disease. *Ann. Neurol.* **53**(Suppl 3), S16–S23.

The Loss of PGAM5 Suppresses the Mitochondrial Degeneration Caused by Inactivation of PINK1 in *Drosophila*

Yuzuru Imai[1*☯], Tomoko Kanao[1☯], Tomoyo Sawada[2], Yoshito Kobayashi[2], Yasuhiro Moriwaki[3], Yosuke Ishida[4], Kohsuke Takeda[4], Hidenori Ichijo[4], Bingwei Lu[5], Ryosuke Takahashi[2]

1 Institute of Development, Aging, and Cancer, Tohoku University, Sendai, Japan, **2** Department of Neurology, Kyoto University Graduate School of Medicine, Kyoto, Japan, **3** Department of Pharmacology, Faculty of Pharmacy, Keio University, Tokyo, Japan, **4** Laboratory of Cell Signaling, Graduate School of Pharmaceutical Sciences, The University of Tokyo, Tokyo, Japan, **5** Department of Pathology, Stanford University School of Medicine, Stanford, California, United States of America

Abstract

PTEN-induced kinase 1 (PINK1), which is required for mitochondrial homeostasis, is a gene product responsible for early-onset Parkinson's disease (PD). Another early onset PD gene product, Parkin, has been suggested to function downstream of the PINK1 signalling pathway based on genetic studies in *Drosophila*. PINK1 is a serine/threonine kinase with a predicted mitochondrial target sequence and a probable transmembrane domain at the N-terminus, while Parkin is a RING-finger protein with ubiquitin-ligase (E3) activity. However, how PINK1 and Parkin regulate mitochondrial activity is largely unknown. To explore the molecular mechanism underlying the interaction between PINK1 and Parkin, we biochemically purified PINK1-binding proteins from human cultured cells and screened the genes encoding these binding proteins using *Drosophila* PINK1 (dPINK1) models to isolate a molecule(s) involved in the PINK1 pathology. Here we report that a PINK1-binding mitochondrial protein, PGAM5, modulates the PINK1 pathway. Loss of *Drosophila* PGAM5 (dPGAM5) can suppress the muscle degeneration, motor defects, and shorter lifespan that result from dPINK1 inactivation and that can be attributed to mitochondrial degeneration. However, dPGAM5 inactivation fails to modulate the phenotypes of *parkin* mutant flies. Conversely, ectopic expression of dPGAM5 exacerbated the *dPINK1* and *Drosophila parkin* (*dParkin*) phenotypes. These results suggest that PGAM5 negatively regulates the PINK1 pathway related to maintenance of the mitochondria and, furthermore, that PGAM5 acts between PINK1 and Parkin, or functions independently of Parkin downstream of PINK1.

Citation: Imai Y, Kanao T, Sawada T, Kobayashi Y, Moriwaki Y, et al. (2010) The Loss of PGAM5 Suppresses the Mitochondrial Degeneration Caused by Inactivation of PINK1 in *Drosophila*. PLoS Genet 6(12): e1001229. doi:10.1371/journal.pgen.1001229

Editor: Juan Botas, Baylor College of Medicine, United States of America

Received May 24, 2010; **Accepted** October 29, 2010; **Published** December 2, 2010

Funding: This work was supported by grants from the Brain Science Foundation, the Suzuken Memorial Foundation, and the Astellas Foundation for Research on Metabolic Disorders, as well as from the Program for Young Researchers from Special Coordination Funds for Promoting Science and Technology commissioned by MEXT and a Grant-in-Aid for Young Scientists (B) from MEXT in Japan (YI). The funders had no role in study design, data collection and analysis, decision to publish, or preparation of the manuscript.

Competing Interests: The authors have declared that no competing interests exist.

* E-mail: yimai@idac.tohoku.ac.jp

☯ These authors contributed equally to this work.

Introduction

Parkinson's disease (PD (OMIM #168600)) is a neurodegenerative disease that affects the maintenance of dopaminergic (DA) neurons. PD prevalence is estimated at ~1% among people over the age of 65 and increases with age. Clinical features of PD include motor abnormalities (tremor, rigidity, akinesia), autonomic disturbances, psychiatric disability and cognitive impairment. The recent identification of PD-associated genes has advanced our understanding the molecular mechanisms underlying PD. Two of these genes, *PINK1* (PARK6, OMIM #605909, Gene ID: 65018) and *parkin* (PARK2, OMIM #600116, Gene ID: 5071), are associated with early-onset autosomal recessive PD, in which loss-of-function (LOF) of a single gene product results in the clinical manifestation of Parkinsonism [1,2]. The *PINK1* gene encodes a serine/threonine kinase with a predicted mitochondrial target sequence and a probable transmembrane domain at the N-terminus [3]. The gene product of the *parkin* gene encodes a protein with an E3 activity [4–6]. Recent genetic studies in *Drosophila* have reported that *dPINK1* (Gene ID: 31607) acts as an upstream regulator of *dParkin* (Gene ID: 40336) in a common pathway that influences mitochondrial maintenance in a subset of tissues, including the flight muscle and DA neurons [7–9]. LOF of the *dPINK1* or the *dparkin* genes results in enlarged or swollen mitochondria, a phenotype that can be partially rescued by heterozygosity for LOF mutations of the mitochondrial fusion-promoting components Optic atrophy 1 (OPA1) and Mitofusin (Mfn), or by increased mitochondrial fission activity via increased dosage of the *dynamin-related protein 1* (*drp1*) gene [10–12]. Studies in mammalian or *Drosophila* cultured cells report that PINK1 is required to recruit Parkin to damaged depolarized mitochondria, and promotes their degradation through an autophagic event called mitophagy [13–16]. Thus, there is strong evidence to support an important role for PINK1 and Parkin in regulating

Author Summary

Parkinson's disease (PD) is a neurodegenerative disease pathologically characterized by degeneration of dopaminergic (DA) neurons in the midbrain. A small percentage of PD cases are inherited in a Mendelian manner, and several disease-causing genes have been identified. The *PINK1* and *Parkin* genes have been isolated as the genes for autosomal recessive form of early-onset PD. Unexpectedly, loss of function of either PINK1 or Parkin in *Drosophila* causes mitochondrial degeneration in the flight muscles, which exhibits a visible phenotype of abnormal wing postures, allowing a rapid genetic screening. We purified PINK1-binding proteins from human cultured cells and screened the gene for these binding proteins using the *PINK1* mutant flies. We found that inactivation of a PINK1-binding protein phosphoglycerate mutase 5 (PGAM5) suppresses mitochondrial degeneration caused by the loss of PINK1 activity. Although *parkin* is suggested to be genetically downstream of *PINK1* in *Drosophila*, loss of PGAM5 failed to modulate the phenotypes by *parkin* inactivation. Our finding suggested that, for mitochondrial maintenance of tissues with high-energy demands such as the muscles and DA neurons, PGAM5 acts between PINK1 and Parkin, or functions independently of Parkin downstream of PINK1.

mitochondrial homeostasis. However, little is known about how PINK1 regulates mitochondrial integrity and turnover through Parkin. Indeed, the precise means by which PINK1 exerts an effect on Parkin is not clear.

Here we show that a mitochondrial protein, phosphoglycerate mutase 5 (PGAM5, Gene ID: 192111), which was previously reported to be localized at the outer mitochondrial membrane and to lack a phosphoglycerate mutase activity [17,18], is involved in the PINK1 pathway, and that loss of PGAM5 activity improves mitochondrial defects caused by PINK1 inactivation in *Drosophila*.

Results

Isolation of PGAM5 as a PINK1-Binding Protein

We and others have previously demonstrated that *PINK1* is genetically upstream of *parkin* [7–9]. To further investigate the relationship between PINK1 and Parkin, we searched for PINK1-binding proteins using a combination of biochemical purification and mass spectrometric analysis. We affinity-purified human PINK1 with a FLAG tag at its C-terminus (hPINK1-FLAG) from lysate of human embryonic kidney (HEK) 293 cells stably expressing hPINK1-FLAG using an anti-FLAG column, and determined proteins specifically presented in the hPINK1-FLAG elution fractions, which include cytoskeleton-related proteins (MAP1B (GeneID: 4131), KIF11 (GeneID: 3832), Tubulin GeneID: 602530, 191130)), proteasome subunits (PSMD1 (GeneID: 5707), PSMD2 (GeneID: 5708), PSMC6 (GeneID: 5706)), PRKDC (GeneID: 5591), Hsp70 (1A, GeneID: 3303; 1B, GeneID: 3304), Hsp90 (GeneID: 3320), Cdc37 (GeneID: 11140), Insulin substrate-4 (IRS-4, GeneID: 8471) and PGAM5 (Figure 1A). PRKDC is one of proteins non-specifically associated with FLAG-tagged proteins in our proteomic analyses (data not shown). The roles of Hsp90, Cdc37 and the proteasome for PINK1 have been characterized previously [15,19–22]. We therefore chose IRS-4 and PGAM5 and tested whether these proteins modulate the *dPINK1* LOF phenotypes by *Drosophila* genetics. Our initial *in vivo* tests revealed that a mutant allele for *dPGAM5* (*CG14816*, GeneID: 31143), $PGAM5^{NP0568}$ significantly suppressed the abnormal wing postures observed in *dPINK1* knockdown flies [9] (Figure 1B), while it failed to improve the viability (Figure 1C). Reducing the dose of *chico* (GeneID: 64880), which encodes a *Drosophila* orthologue of IRS-4, significantly suppresses the short lifespan phenotype caused by *dPINK1* knockdown, without affecting wing posture (Figure 1D and 1E). Inhibition of *chico* activity has previously been reported to extend the lifespan of *Drosophila*, such that we reasoned that the effect on lifespan we observed might reflect a general phenomenon rather than reflecting a specific interaction with *dPINK1* [23]. Thus for subsequent studies, we chose to focus on PGAM5.

The results of co-immunoprecipitation confirmed that C-terminally Myc-tagged human PGAM5 (hPGAM5-Myc) specifically binds to hPINK1-FLAG in transfected HEK293 cells (Figure 2A). Moreover, we found that hPGAM5 and hPINK1 immunoreactivity co-localizes with mitochondria in transfected HeLa cells, consistent with the previous finding that PGAM5 is localized to the mitochondria (Figure 2B and 2C) [24]. To test if endogenous hPGAM5 interacts with hPINK1, we first generated an anti-hPGAM5 antibody (Figure 2D). Next, we used a previously established anti-PINK1 antibody to immunoprecipitate PINK1 from HEK293 cell lysate, then probed with anti-PGAM5 to detect endogenous hPGAM5. As shown in Figure 2E, endogenous hPGAM5 was detectable in the fraction immunoprecipitated using anti-hPINK1 antibody but not a control antibody, confirming the results of mass spectrometric analysis. Physical association of dPINK1 with dPGAM5 was also observed in *Drosophila* S2 cells (Figure 2F), suggesting that their functional interaction is conserved between human and *Drosophila*.

Previous findings that PINK1 and PGAM5 possess kinase and phosphatase activities, respectively [18,25,26], prompted us to test the possibility of their enzyme-substrate relationships. A mobility shift assay to monitor the status of PINK1 phosphorylation suggested that overexpression of hPGMA5 has little effect on hPINK1 phosphorylation (Figure 2G). On the other hand, an *in vitro* kinase assay using recombinant dPINK1 failed to show a possibility that PGAM5 is a substrate for PINK1, or that PGAM5 modifies hPINK1 kinase activities (Figure 2H).

dPGAM5 Alters Mitochondrial Morphology in *Drosophila*

The *Drosophila* genome appears to have two orthologs of mammalian *PGAM5*, one on the X (*CG14816*) and the other on the second chromosome (*CG15874*, GeneID: 37899). We have renamed *CG14816* and *CG15874* as *dPGAM5* and *dPGAM5-2*, respectively. Our initial *in vivo* genetic study and most subsequent analyses were performed using *dPGAM5* mutant and transgenic animals because *dPGAM5* is more similar to *hPGAM5* than is *dPGAM5-2* (*dPGAM5 vs. hPGAM5*, 44% amino acid identity, and *dPGAM5-2 vs. hPGAM5*, 38% identity, as determined using ClustalW v1.4 to align the sequences), and because the results of high-throughput analysis of transcript abundance suggest that the *dPGAM5-2* transcript is expressed at very low levels at the adult stage, if at all (see http://flybase.org/reports/FBgn0035004.html).

We determined the *P*-element insertion allele $PGAM5^{NP0568}$ as a hypomorph allele, which showed a reduction of *dPGAM5* transcript levels to about 25% of normal levels (Figure S1). We then generated a *dPGAM5* null allele $PGAM5^{1}$, in which the expression of dPGAM5 completely disappeared at both the transcript and protein levels (Figure S1B and S1C). The $PGAM5^{1}$ homozygous animal is viable, fertile and grossly normal. However, it displayed longer lifespan (Figure 3A). By contrast, overexpression of dPGAM5 or dPGAM5-2 resulted in shorter longevity (Figure 3B). Since a previous report described that overexpression of human PGAM5 affects the mitochondrial morphology or

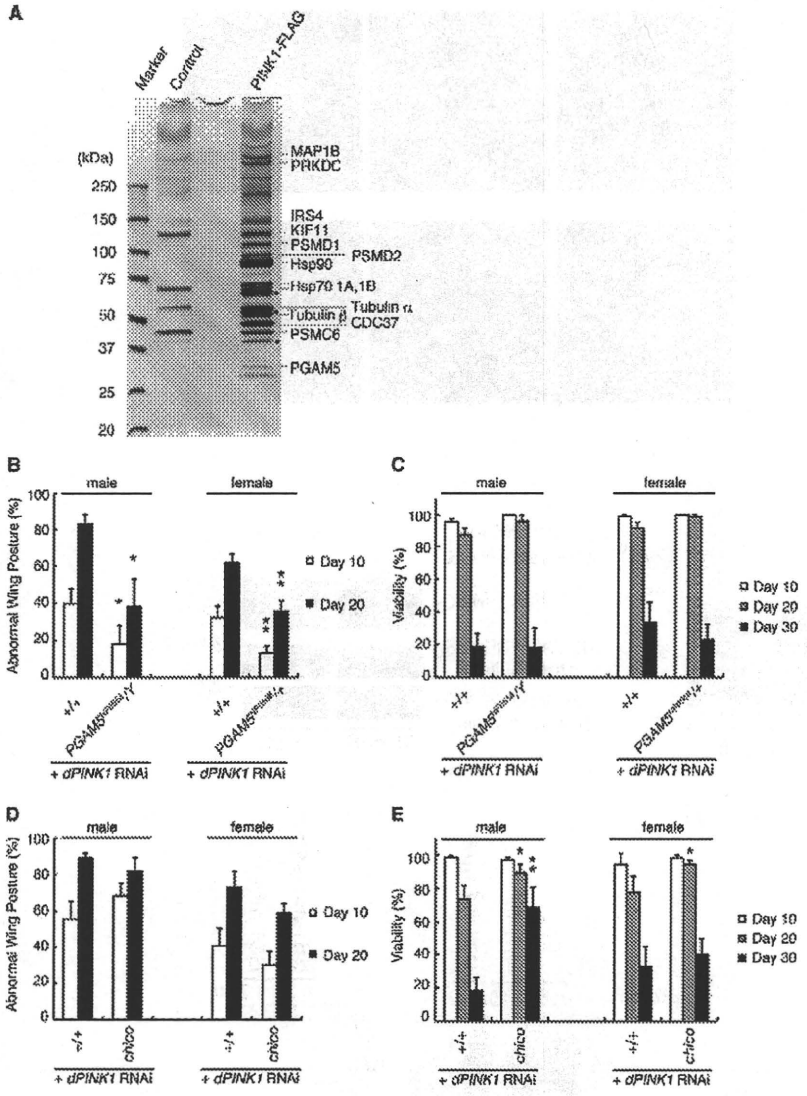

Figure 1. Identification of PINK1-binding proteins that modulate the phenotypes of *dPINK1* knockdown fly. (A) Silver-stained polyacrylamide gel to visualize hPINK1-binding proteins. FLAG elution fractions purified from cells stably expressing hPINK1-FLAG (PINK1-FLAG lane) and parental cells (Control lane) are separated on a gel (For details of the procedure, see Materials and Methods). Bands corresponding to hPINK1 (dots) and representative co-purified proteins are indicated. (B, C) The wing phenotype typical of 10- and 20-day-old *dPINK1* RNAi flies [9] (B) was suppressed by the $PGAM5^{NP0568}$ mutant allele, whereas viability of 10-, 20- and 30-day-old adult flies was not improved (C). *, $p<0.05$; **, $p<0.01$ *vs.* age-matched *dPINK1* RNAi group in Student's *t*-test. The genotypes are as follows: *MHC-GAL4>* $dPINK1^{RNAi}$ (+/+), $PGAM5^{NP0568}$*/Y; MHC-GAL4>* $dPINK1^{RNAi}$ ($PGAM5^{NP0568}$*/Y*), $PGAM5^{NP0568}$*/+; MHC-GAL4>* $dPINK1^{RNAi}$ ($PGAM5^{NP0568}$*/+*). *MHC-GAL4*, a muscle-specific driver. Flies were raised at 29°C as the RNAi-induced dPINK1 defects are more pronounced when flies are raised at that temperature. (D, E) Removal of one copy of the *IRS4* ortholog *chico* had no effect on the wing phenotype of *dPINK1* RNAi flies (D) but improved viability (E). *, $p<0.05$; **, $p<0.01$ *vs.* age-matched *dPINK1* RNAi group. The genotypes are: *MHC-GAL4>* $dPINK1^{RNAi}$ (+/+), *chico/+; MHC-GAL4>* $dPINK1^{RNAi}$ (*chico*). Flies were raised at 29°C.
doi:10.1371/journal.pgen.1001229.g001

mobility in the cultured cells [24], we observed the mitochondria in the *dPGAM5* null and transgenic flies. Although inactivation of *dPGAM5* gene function did not cause mitochondrial degeneration, the morphology of the mitochondria appears to be moderately altered (Figure 3D and 3H compared to Figure 3C and 3G). The mitochondria in the indirect flight muscles of the *PGAM5* mutant flies were longer in the long-axis direction compared to control animals (Figure 3K). A similar tendency was seen in DA neurons of the adult brain although the difference did not reach statistical significance (Figure 3L and 3M). In addition, we frequently observed constrictions in the mitochondria (see broken lines in Figure 3D). In contrast, transgenic expression of dPGAM5 or dPGAM5-2 in *Drosophila* leads to fragmentation of mitochondria, with cristae well-preserved in the indirect flight muscles (Figure 3E, 3F, 3I, and 3J) and in the tyrosine-hydroxylase (TH)-positive neurons of the adult fly brain (Figure 3N and 3O). These results suggested that dPGAM5 is likely to promote the mitochondrial fission process in *Drosophila*.

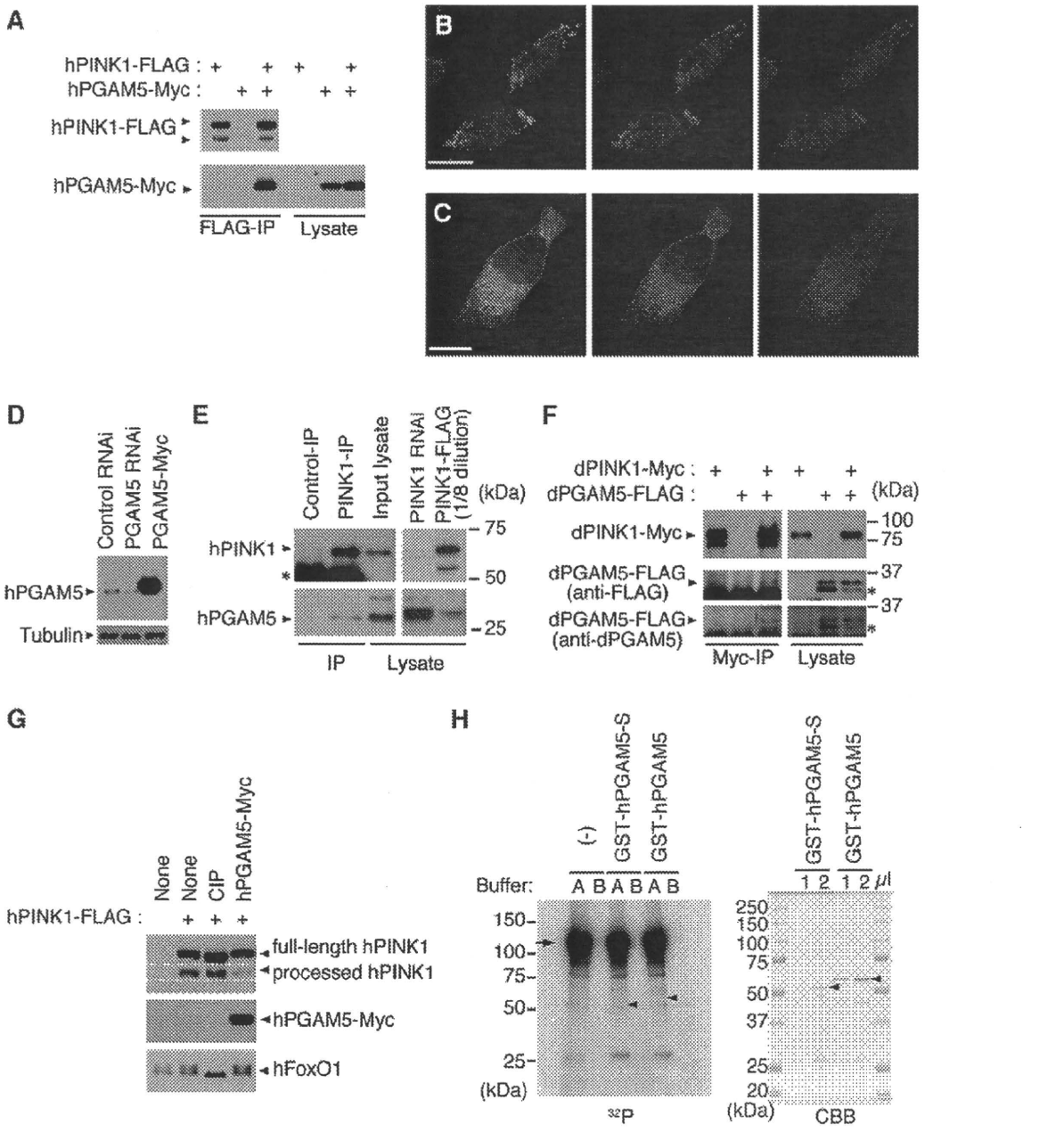

Figure 2. PGAM5 associates with PINK1 at mitochondria. (A) hPGAM5 binds to hPINK1 in HEK293 cells. Lysate expressing C-terminally Myc-tagged hPGAM5 (hPGAM5-Myc) and FLAG-tagged hPINK1 (hPINK1-FLAG) was subjected to immunoprecipitation with anti-FLAG antibody (FLAG-IP), and analyzed by immunoblotting with anti-tag antibodies. (B) hPGAM5 is localized to the mitochondria. HeLa cells transfected with hPGAM5-Myc were visualized with anti-Myc (green). Mitochondria were visualized with MitoTracker (red) and nuclei with DAPI (blue). Regions of co-localization of hPGAM5 with mitochondria appear in yellow in the merged image. (C) hPGAM5 and hPINK1 co-localize at mitochondria. HeLa cells co-transfected with hPINK1 and hPGAM5-Myc were stained with anti-PINK1 (green) and anti-Myc (red). (D) Anti-hPGAM5 antibody specifically recognizes ~30 kDa bands in extract from HEK293 cells, which were reduced in lysates from cells treated with siRNAs directed against hPGAM5. Lysate expressing hPGAM5-Myc and anti-tubulin signals served as a positive control and a loading control, respectively. (E) Endogenous hPGAM5 is associated with hPINK1. An anti-PINK1 (PINK1-IP) or an antibody against the unrelated protein Delta (Control-IP) was used for immunoprecipitation of proteins in HEK293 cells. Cell lysate in which hPINK1 was knocked down by RNAi (PINK1 RNAi) and lysate from cells that overexpressed hPINK1-FLAG (PINK1-FLAG) served as additional controls. The PINK1-FLAG lysate was diluted eight-fold with loading buffer to reduce the strong signal present in that sample. Asterisk, bands attributable to detection of the antibodies themselves, which may mask lower molecular weight hPINK1 bands (~52 kDa). (F) dPGAM5 is associated with dPINK1 in *Drosophila* S2 cells. S2 cell lysate expressing dPINK1-Myc and dPGAM5-FLAG was subjected to immunoprecipitation with anti-Myc antibody (Myc-IP), and analyzed by immunoblotting with anti-tag or anti-dPGAM5 antibodies. Asterisks, a putative processed form of dPGAM5. (G) HEK 293 cell lysate expressing hPINK1-FLAG together with hPGAM5-Myc was subjected to Phos-tag immunoblotting [43]. hPINK1-FLAG lysate treated with alkaline phosphatase (CIP) was used as a positive control. A phospho-protein FoxO1 was efficiently dephosphorylated by the CIP treatment. (H) An *in vitro* kinase assay was performed using 2x GST-dPINK1 and GST-hPGAM5. Recombinant

2x GST-dPINK1 purified from bacteria was used as a kinase source. Recombinant GST-hPGAM5 short form (GST-hPGAM5-S) or GST-hPGAM5 was purified from bacteria and 1 and 2 μl of the purified fractions were separated by SDS-PAGE and stained with Coomassie Brilliant Blue (CBB, right-hand panel; arrowheads, GST-hPGAM5-S or GST-hPGAM5). A total of 100 or 400 ng of GST-hPGAM5-S or GST-hPGAM5, respectively, were incubated with 100 ng of 2x GST-dPINK1 in kinase reaction buffer A (100 mM Tris-HCl [pH 7.5], 240 mM NaCl, 30 μM ATP, 10 mM $MgCl_2$, 2 mM $CaCl_2$, 5 μCi γ-^{32}P ATP) or buffer B (100 mM Tris-HCl [pH7.5], 240 mM NaCl, 30 μM ATP, 10 mM EDTA, 5 μCi γ-^{32}P ATP) for 30 min at 30°C. The reaction mixture was suspended in SDS sample buffer and then subjected to SDS-PAGE and autoradiography (Left, ^{32}P; the arrow and arrowheads represent expected migration positions of 2x GST-dPINK1 and GST-hPGAM5/GST-hPGAM5-S, respectively). No specific signals corresponding hPGAM5 or hPGAM5-S were observed. Note that 2x GST-dPINK1 lacks kinase activity in the buffer B, suggesting that activation of PINK1 requires divalent cations such as Mg^{2+} and Ca^{2+}. Scale bars = 15 μm in (B and C).
doi:10.1371/journal.pgen.1001229.g002

The Relationship between PGAM5 and the Mitochondrial Fission/Fusion Machinery

Evolutionarily-conserved GTPases Mfn and OPA1 promote the mitochondrial fusion event while another GTPase Drp1 regulates the mitochondrial fission [27,28]. To determine the role of PGAM5 in the mitochondrial fission pathway, we manipulated the activities of the genes that are involved in mitochondrial fission/fusion in *dPGAM5* null flies. Decreased Mfn activity resulted in fragmented mitochondria in the indirect muscle tissues, which was not affected by removal of the *dPGAM5* gene (Figure 4A–4D and 4G, Figure S2). Conversely, an increased mitochondrial fission activity by introducing an extra copy of the *drp1* gene was not suppressed in the *dPGAM5* null genetic background (Figure 4E–4G). These results suggested that dPGAM5 may function upstream of Mfn or Drp1, or that the mechanism of the mitochondrial morphological changes by dPGAM5 is independent of that of the known fusion/fission components.

dPGAM5 Modulates Phenotypes Caused by *dPINK1* Inactivation in *Drosophila*

We next confirmed that the results of the genetic tests in Figure 1B and 1C using a LOF allele for *dPINK1*, $PINK1^{B9}$ to exclude off-target effects due to RNAi (Figure 5). Adult $PINK1^{B9}$ flies often have abnormal thoraces with dents in the mid-anterior region, which is likely due to degeneration of the muscle tissues lining the inside of the thorax (Figure 5B) [8]. This thorax phenotype seen in $PINK1^{B9}$ flies can be suppressed by introduction of the $PGAM5^{NP0568}$ or the $PGAM5^{1}$ allele (Figure 5A and 5D). We then examined the effects of *dPGAM5* inactivation on *dPINK1* mutant phenotypes that progressively increase over time. As described above, loss of *dPINK1* activity leads to the appearance of abnormal wing postures, which is indicative of flight muscle degeneration, and the percent of affected flies increases with advancing age (Figure 5C and 5F) [8]. Introduction of the *dPGAM5* mutant alleles dramatically suppresses this phenotype (Figure 5E and 5F), whereas ectopic expression of dPGAM5 enhances the phenotype (Figure 5G). Progressive loss of climbing ability and the shorter lifespan of $PINK1^{B9}$ flies are additional prominent phenotypes that may represent dysfunction of DA neurons of the central nervous system and muscle degeneration. The *dPGAM5* mutant alleles also significantly improved these phenotypes (Figure 5H and 5J). Conversely, overexpression of dPGAM5 worsened the phenotypes (Figure 5I and 5K). Transmission electron microscopy (TEM) sections from one day-old adult $PINK1^{B9}$ mutant flies reveal that mitochondria in the indirect flight muscles are abnormally fused with one another and that the structures of the mitochondrial cristae are unclear (*i.e.* the cristae have lost the normal electron density seen by TEM) as compared to those of a *dPINK1* revertant line (Figure 6A and 6D compared to Figure 3C and 3G). Importantly, the mitochondrial hyperfusion and loss of cristae usually observed in *dPINK1* mutant animals can be partly suppressed by introduction of the $PGAM5^{NP0568}$ or the $PGAM5^{1}$ allele (Figure 6B, 6E, and 6G). In sharp contrast, transgenic expression of dPGAM5 further promoted mitochondrial degeneration (Figure 6C and 6F). Similar results were obtained when mitochondria in DA neurons of the adult brain (Figure 6H, 6I, and 6J) and in the indirect muscle tissues (Figure S3) were visualized using a version of GFP with a mitochondrial targeting signal (mitoGFP). Mitochondrial morphology in DA neurons in wild-type flies showed a long tubular network in the cytoplasm (Figure 3L). As previously reported, DA neurons in $PINK1^{B9}$ flies form spherical aggregates of mitochondria (Figure 6I). Removal of *dPGAM5* from $PINK1^{B9}$ flies led to an increase in the number of small fragmented or tubular mitochondria (Figure 6J). These results suggest that excessive mitochondrial aggregation, which is modulated by dPGAM5 inactivation, is indicative of a functional failure of mitochondria in DA neurons.

Consistent with the beneficial effects of dPGAM5 inactivation on the mitochondrial degeneration seen in $PINK1^{B9}$ flies, we observed that dPGAM5 inactivation suppresses the loss of DA neurons in the protocerebral posterior lateral 1 (PPL1) and protocerebral posterior medial 1 and 2 (PPM1/2) clusters of aged flies (Figure 6K–6M).

Removal of *dPGAM5* Fails to Suppress Phenotypes Resulting from *dparkin* Inactivation

Previous studies in *Drosophila* suggested that *dPINK1* is genetically associated with *dparkin* and furthermore, that *dPINK1* functions upstream of *dparkin* [7–9]. In addition, *dparkin* null mutations cause mitochondrial degeneration of a subset of tissues in *Drosophila*, which phenocopies dPINK1 inactivation [29,30]. Given the evidence that PGAM5 is involved in the PINK1 pathway, we next asked if dPGAM5 also affects the *in vivo* mitochondrial phenotypes associated with mutations in *dParkin*. Introduction of $PGAM5^{NP0568}$ in the *parkin* hypomorphic genetic background ($parkin^{P21}$) had little effect on abnormal wing postures (Figure 7A–7C) [29,30]. Consistent with the result in the wing phenotype, loss of *dPGAM5* activity failed to rescue the age-dependent motor defects and shorter lifespan observed in $parkin^{P21}$ flies (Figure 7D and 7F). In the same settings, overexpression of dPGAM5 further enhanced both motor defect and reduced lifespan phenotype (Figure 7E and 7G). Loss of dParkin activity results in an elongated morphology in mitochondria of the adult indirect flight muscle tissues, a phenotype that was suppressed by loss of the *dPGAM5* gene (Figure 7H, 7I, and 7L). However, the crista structures of the mitochondria were not restored by inactivation of the *dPGAM5* gene (Figure 7J and 7K). Taken together, these data suggest that *dPGAM5* lies genetically upstream of *dparkin*, or functions independently of *dparkin* downstream of *dPINK1* in *Drosophila*.

Activation of a Redox Control Pathway Improves Viability of *dPINK1* Mutant Flies

PGAM5 was previously reported to interact with Keap1 (Gene ID: 9817), a substrate adaptor protein for a Cullin-3-dependent E3

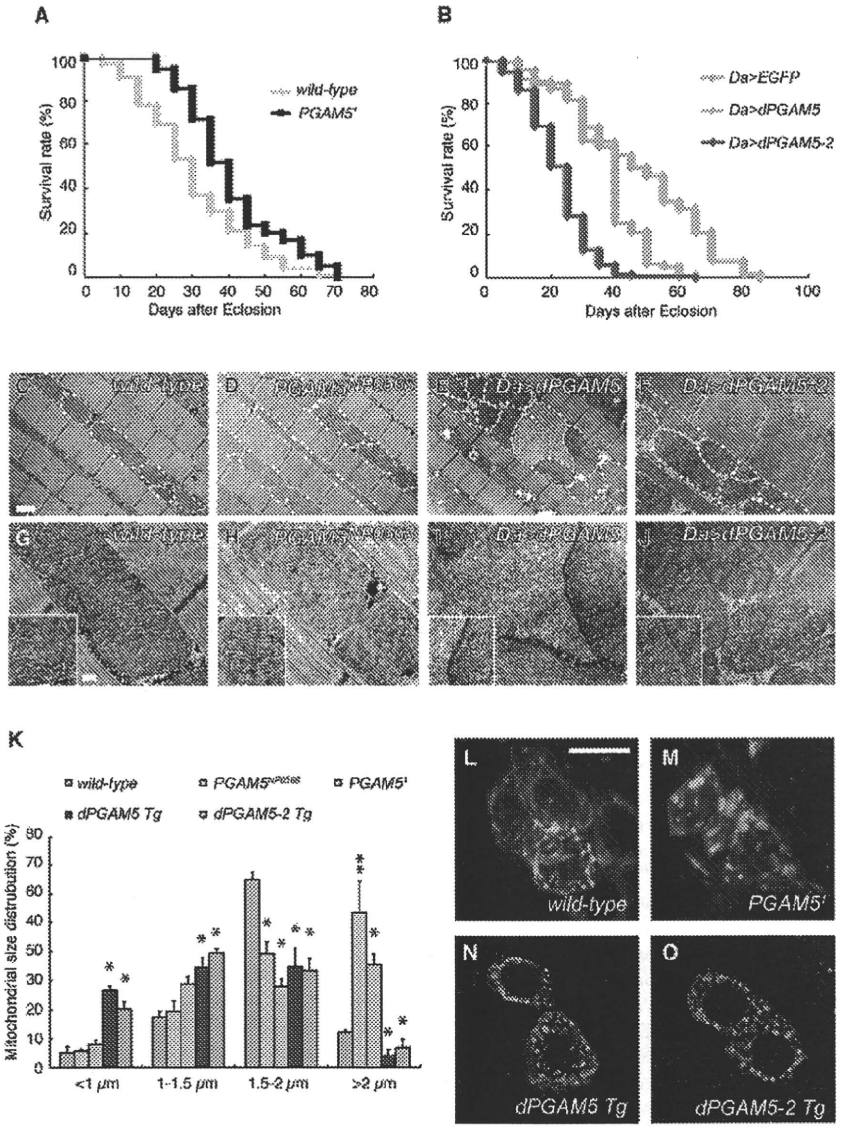

Figure 3. dPGAM5 is dispensable for normal development, but affects lifespan in *Drosophila*. (A) Loss of dPGAM5 genes extends the lifespan. Adult male *wild-type* (*yw/Y*; $n = 125$) *vs. dPGAM5 null* (*y, PGAM5*^{1}*/Y*; $n = 125$) flies, $p<0.001$ by log rank test. (B) Overexpression of *dPGAM5* or *dPGAM5-2* in *Drosophila* causes shorter lifespan. Overexpression of the transgenes was induced using the ubiquitous *daughterless* (*Da*)-*GAL4* driver. Lifespan of adult male *EGFP* ($n = 130$), *dPGAM5* ($n = 76$) and *dPGAM5-2* ($n = 117$) flies. *EGFP vs. dPGAM5*, $p<0.001$; *EGFP vs. dPGAM5-2*, $p<0.001$; by log rank test. (C–J) Transmission electron microscopy (TEM) analysis of the indirect flight muscle and morphology of mitochondria in 2-day-old adult flies with the indicated genotypes. In C–F, we outlined some mitochondria with broken lines to highlight morphology. The insets in G–J show representative mitochondria matrixes. A revertant, *PINK1*^{RV}, was used as a wild-type comparison [8]. The genotypes are: *PINK1*^{RV}*/Y* (C, G), *PGAM5*^{NP0568}*/Y* (D, H), *Da-GAL4> UAS-dPGAM5* (E, I), *Da-GAL4> UAS-dPGAM5-2* (F, J). Scale bars = 1 μm in C–F and 200 nm in G–J. (K) Quantification of the percentage of mitochondrial size distribution in the indirect muscle tissue from *wild-type* ($n = 136$ from 5 adult flies), *PGAM5*^{NP0568} ($n = 155$ from 5), *PGAM5*^{1} ($n = 87$ from 5), *dPGAM5 Tg* ($n = 143$ from 5) and *dPGAM5-2 Tg* flies ($n = 147$ from 5) as shown in (C–J). The length of the mitochondria in the direction of the myofibrils was measured. Data are shown as means ± SE (* $p<0.05$, ** $p<0.01$ *vs. wild-type*). (L–O) Brain tissues of 5-day-old adult flies were stained with anti-TH antibody (red). Mitochondria labeled with mitoGFP (green) were observed in the PPL1 TH-positive neurons of the indicated genotypes. The genotypes are as follows: *TH-GAL4> mitoGFP* (*wild-type*), *PGAM5*^{1}*/Y; TH-GAL4>UAS-mitoGFP* (*PGAM5*^{1}), *UAS-dPGAM5/TH-GAL4> UAS-mitoGFP* (*dPGAM5 Tg*), *UAS-dPGAM5-2/TH-GAL4> UAS-mitoGFP* (*dPGAM5-2 Tg*). *TH-GAL4*, a DA neuron-specific driver. Scale bar = 5 μm.
doi:10.1371/journal.pgen.1001229.g003

complex [17]. In a normal redox state, the Keap1 complex suppresses activity of a bZIP transcription factor, Nrf2, through ubiquitin/proteasome-dependent protein degradation [31]. Oxidative stress impairs inhibition of Nrf2 by Keap1 [31]. Nrf2 thus becomes stabilized and activates oxidative stress protective genes, restoring cellular redox homeostasis. Although we confirmed the association of PGAM5 with Keap1 in human cultured cells, the proposed Keap1-binding motif in PGAM5, N*X*ESGE, was not conserved in dPGAM5 (Figure S1). On the other hand, Keap1/Nrf2 signaling does appear to be conserved in *Drosophila* [32]. We

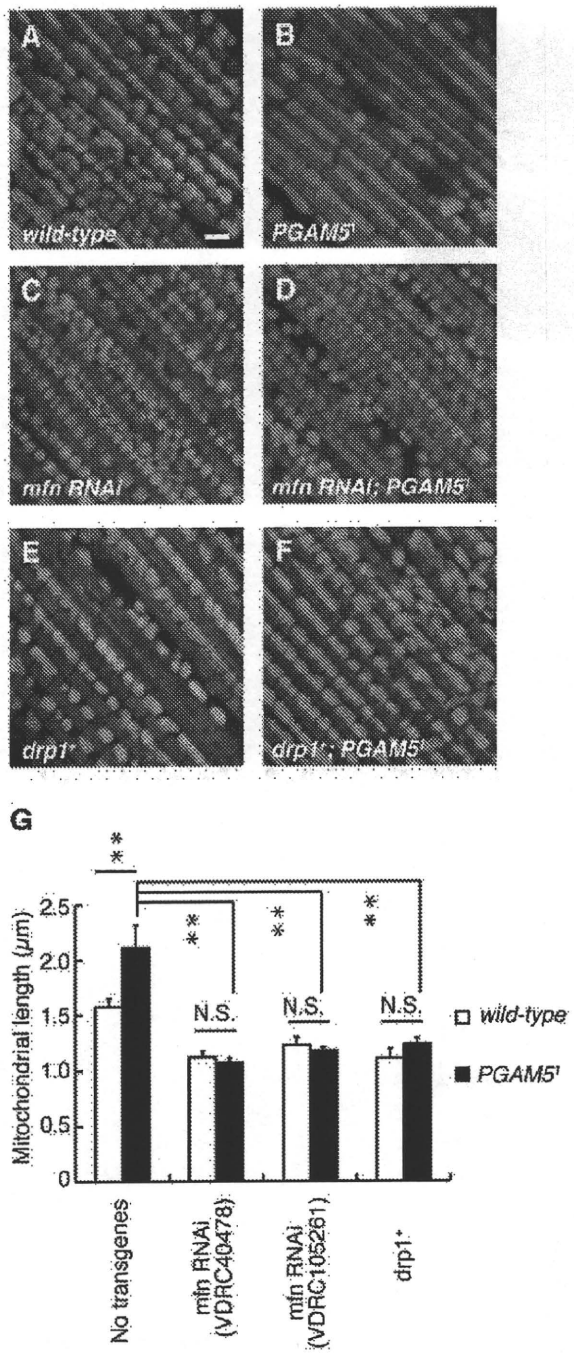

Figure 4. Relationship between *dPGAM5* and the mitochondrial fusion/fission genes. (A–F) dPGAM5 inactivation failed to rescue the mitochondrial fragmentation caused by *mfn* knockdown (*mfn RNAi*) or introduction of an extra copy of the *drp1* gene ($drp1^+$). To visualize the mitochondria under a fluorescence microscopy, we used the muscle-specific *MHC-GAL4* driver to induce expression of a mitoGFP (green) transgene in 5-day-old adult flies with the indicated genotypes. Muscle tissue was counterstained with phalloidin (red). Scale bar = 2 μm. (G) The average length of the mitochondria in the direction of the myofibrils was measured from *wild-type* ($n = 343$ from 7 adult flies), $PGAM5^1$ ($n = 390$ from 8), *mfn RNAi* (VDRC40478, $n = 305$ from 6; VDRC105261, $n = 372$ from 8), *mfn RNAi* (VDRC40478); $PGAM5^1$ ($n = 355$ from 7), *mfn RNAi* (VDRC105261); $PGAM5^1$ ($n = 237$ from 5), $drp1^+$ ($n = 245$ from 5) and $drp1^+$; $PGAM5^1$ ($n = 247$ from 5) as shown in (A–F). Data are shown as means ± SE (**$p < 0.01$; N.S., not significant). The genotypes are as follows: *+/Y; MHC-GAL4>mitoGFP* (A, *wild-type*), $PGAM5^1$*/Y; MHC-GAL4>UAS-mitoGFP* (B, $PGAM5^1$), *+/Y; MHC-GAL4>UAS-mitoGFP; UAS-mfn RNAi* (VDRC40478) (C, *mfn RNAi*), $PGAM5^1$*/Y; MHC-GAL4>UAS-mitoGFP; UAS-mfn RNAi* (VDRC40478) (D, *mfn RNAi*; $PGAM5^1$), *+/Y; MHC-GAL4>mitoGFP;* $drp1^+$ (E, $drp1^+$), $PGAM5^1$*/Y; MHC-GAL4>mitoGFP;* $drp1^+$ (F, $drp1^+$; $PGAM5^1$).
doi:10.1371/journal.pgen.1001229.g004

tested if Keap1/Nrf2 signaling modulates *PINK1* phenotypes. Removal of a copy of the *keap1* gene (Gene ID: 42062) in *dPINK1* knockdown flies, wherein the *dPINK1* RNAi was expressed in the muscle tissues, failed to rescue the abnormal wing posture (Figure 8A). However, *Keap1* heterozygosity is beneficial to survival of aging *dPINK1* knockdown files, supporting a previous report suggesting that oxidative stress is partly involved in the PINK1 pathology (Figure 8B) [33,34].

Discussion

The event of fusion/fission is required for maintenance of a healthy mitochondrial population. Mitochondrial fusion is believed to require the interchange of a set of internal components, including copies of the mitochondrial genome, respiratory proteins and metabolic products. Mitochondrial fission has been proposed to play a role in disposal of damaged mitochondria, such as those with a reduced mitochondrial membrane potential, via mitophagy [35]. A role for PINK1 in the regulation of mitochondrial fission/fusion dynamics has recently been demonstrated in *Drosophila* [10–12]. The PINK1/Parkin pathway appears to promote fission and/or inhibits fusion, likely through an indirect mechanism. Indeed, loss of dPINK1 or dParkin produces swollen or enlarged mitochondria in tissues with high-energy demands, such as the muscles, which is suppressed by reduced fusion activity or increased fission activity after genetic manipulation of the mitochondrial fission/fusion machinery. Namely, either reducing the activity of the mitochondrial fusion proteins OPA1 and Mfn, or increasing the activity of a mitochondrial fission protein, Drp1, can partially rescue *PINK1* and *parkin* mutant phenotypes.

We identified PGAM5 as a PINK1-binding protein and went on to show that *dPGAM5* can modulate *dPINK1* mutant phenotypes. Loss of *dPGAM5* activity had little effect on the lifespan of a *dPINK1* RNAi fly strain in our initial *in vivo* test (Figure 1C). However, we found that loss of *dPGAM5* does significantly extend lifespan of $PINK1^{B9}$ mutant flies (Figure 5J). We speculate that continuous expression of the short hairpin RNA in the RNAi-based test confers additional toxicity, leading to a shorter lifespan in a sequence-independent manner, such that the suppressive effect of *dPGAM5* mutations cannot be detected in the *PINK1* RNAi flies.

dPGAM5 appears to be dispensable for mitochondrial homeostasis in *Drosophila*, as overall, flies homozygous for a null allele of *dPGAM5*, $PGAM5^1$, appear to be normal. It has previously been reported that ectopic expression of PGAM5 leads to perinuclear aggregation or small fragmentation of mitochondria in mammalian cultured cells, which suggested that PGAM5 has a role in regulation of mitochondrial fission/fusion process or mobility [24]. Our study also observed alteration of mitochondrial morphology in *Drosophila* with different dPGAM5 activities. Transgenic expression of dPGAM5 or dPGAM5-2 leads to fragmentation of mitochondria both in the TH^+ neurons and indirect flight muscles (Figure 3E, 3F, 3I and 3J). By contrast, dPGAM5 LOF moderately increases mitochondria with a longer tubular or a swollen morphology (Figure 3D and 3K). Our genetic tests with the

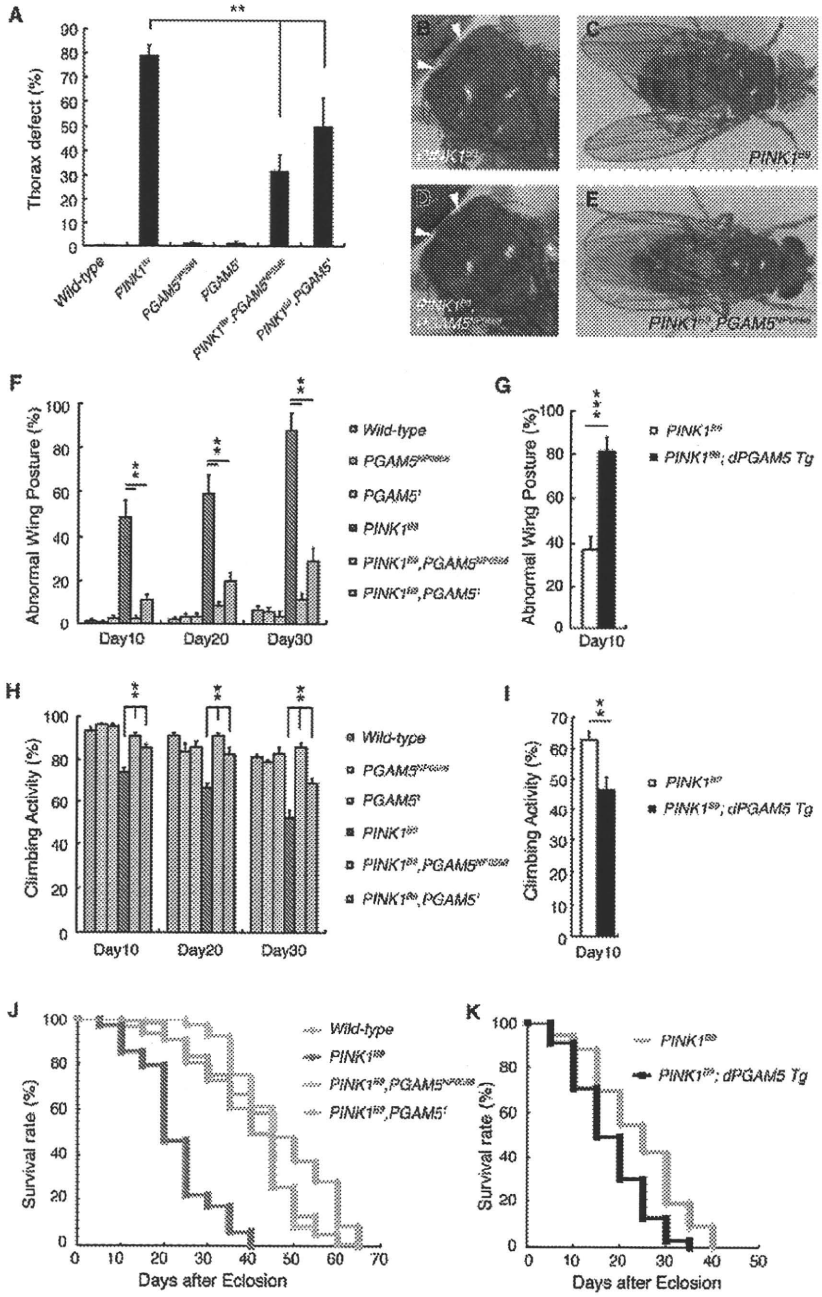

Figure 5. Loss of *dPGAM5* suppresses *dPINK1* mutant phenotypes in *Drosophila*. A thorax defect (B, arrowheads) and abnormal wing posture (C) caused by loss of *dPINK1* activity are suppressed in *dPGAM5* mutant genetic backgrounds (A, D and E). (F) Percentage of 10-, 20- and 30-day-old male flies showing abnormal wing postures. Error bars show S.E. from three experiments. (G) Percentage of 10-day-old male $PINK1^{B9}$ and $PINK1^{B9}$ ubiquitously overexpressing *dPGAM5* flies showing abnormal wing postures. Error bars show S.E. from three experiments. (H, I) Percentage of locomotor activity. Error bars show S.E. from three repeated experiments. (J) Lifespan of adult male flies. Loss of *dPGAM5* partially improved the reduced lifespan seen in $PINK1^{B9}$ fly ($PINK1^{B9}$ *vs.* $PINK1^{B9}$, $PGAM5^{NP0568}$ or $PINK1^{B9}$, $PGAM5^{1}$, $p<0.001$; *wild-type vs.* $PINK1^{B9}$, $PGAM5^{NP0568}$ or $PINK1^{B9}$, $PGAM5^{1}$, $p<0.01$ by the log rank test). (K) Lifespan of adult male $PINK1^{B9}$ and $PINK1^{B9}$ ubiquitously overexpressing *dPGAM5* flies. Overexpression of dPGAM5 further reduced the lifespan ($PINK1^{B9}$ *vs.* $PINK1^{B9}$; *dPGAM5 Tg*, $p<0.001$). The same files were used in (A–F, H and J) and in (G, I and K). The genotypes and the number used in the assays are; *wild-type* ($PINK1^{RV}/Y$, $n=161$), $PGAM5^{NP0568}$ ($PGAM5^{NP0568}/Y$, $n=161$), $PGAM5^{1}$ ($PGAM5^{1}/Y$, $n=161$), $PINK1^{B9}$ ($PINK1^{B9}/Y$, $n=101$), $PINK1^{B9}$, $PGAM5^{NP0568}$ ($PINK1^{B9}$, $PGAM5^{NP0568}/Y$, $n=162$) and $PINK1^{B9}$, $PGAM5^{1}$ ($PINK1^{B9}$, $PGAM5^{1}/Y$, $n=160$) in (A–F, H and J), $PINK1^{B9}$ ($PINK1^{B9}/Y$; *Da-GAL4/+*, $n=162$) and $PINK1^{B9}$, *dPGAM5 Tg* ($PINK1^{B9}/Y$; *Da-GAL4> UAS-dPGAM5*, $n=161$) in (G, I and K).
doi:10.1371/journal.pgen.1001229.g005